JGR Oceans

RESEARCH ARTICLE
10.1029/2025JC023417

Autonomous Float Data Reveal Decoupled Trends in Chlorophyll and Stratification in the Indian Ocean

Marufa Ishaque[1,2], **Sophie Clayton**[2,3], **and John Klinck**[2]

[1]Jet Propulsion Laboratory, California Institute of Technology, Pasadena, CA, USA, [2]Department of Ocean and Earth Sciences, Old Dominion University, Norfolk, VA, USA, [3]Marine Biogeochemistry, National Oceanography Center, Southampton, UK

Key Points:

- Depth-integrated chlorophyll and NPP have increased in the Bay of Bengal and western Arabian Sea, but decreased in the eastern Arabian Sea
- There is no strong positive or negative correlation between stratification and depth-integrated chlorophyll or NPP
- A weak negative correlation exists between depth-integrated chlorophyll and NPP and IOD/ENSO indices in most of the northern Indian Ocean

Supporting Information:

Supporting Information may be found in the online version of this article.

Correspondence to:

M. Ishaque,
marufa.ishaque@jpl.nasa.gov

Citation:

Ishaque, M., Clayton, S., & Klinck, J. (2026). Autonomous float data reveal decoupled trends in chlorophyll and stratification in the Indian Ocean. *Journal of Geophysical Research: Oceans*, *131*, e2025JC023417. https://doi.org/10.1029/2025JC023417

Received 9 SEP 2025
Accepted 4 APR 2026

Author Contributions:

Conceptualization: Marufa Ishaque, Sophie Clayton, John Klinck
Data curation: Marufa Ishaque
Formal analysis: Marufa Ishaque
Funding acquisition: Sophie Clayton, John Klinck
Investigation: Marufa Ishaque
Methodology: Marufa Ishaque, Sophie Clayton, John Klinck
Project administration: Sophie Clayton, John Klinck
Resources: Marufa Ishaque
Software: Marufa Ishaque
Supervision: Sophie Clayton, John Klinck

Abstract Recent studies have shown that the Indian Ocean is warming significantly, but how this warming impacts primary production is largely unresolved due to a relative lack of depth-resolved biological observations. In this study, we have used Biogeochemical-Argo data from 2013 to 2022, comprising over 9,000 individual profiles, to examine regional patterns and trends in depth-integrated chlorophyll, depth-integrated net primary production and stratification in the northern and Equatorial Indian Ocean. Our analysis shows that water column stratification is increasing in the majority of the study area, with the highest rate of increase observed in the western Bay of Bengal. At the same time, we find that depth-integrated chlorophyll and depth-integrated net primary production show an increasing trend in most parts of the Bay of Bengal, the western Arabian Sea, and some parts of the Equatorial Indian Ocean. However, the eastern Arabian Sea, the northern Bay of Bengal, and other parts of the Equatorial Indian Ocean have experienced a decrease in depth-integrated chlorophyll and net primary production. The Indian Ocean Dipole and El Niño Southern Oscillation were found mostly to be weakly negatively correlated with the depth-integrated chlorophyll and depth-integrated net primary production in the northern Indian Ocean. Our results show that depth-integrated chlorophyll and depth-integrated net primary production are not strongly or consistently correlated with stratification within our study region, suggesting that the projected increases in stratification with ocean warming in this region may not drive concurrent reductions in primary production.

Plain Language Summary It is widely believed that increased upper ocean warming will result in decreased primary production. The Indian Ocean has experienced significant warming over recent years; however, a relative lack of water column measurements of chlorophyll has hampered our ability to determine relationships between productivity and thermal stratification driven by warming. Thanks to the global Biogeochemical-Argo program, which deploys autonomous floats equipped with biogeochemical sensors that measure chlorophyll as well as a host of other ocean variables, we have 10 years of data from the northern Indian Ocean to determine the relationship between chlorophyll, net primary production and stratification in this basin. Our analysis shows that there is no strong correlation between depth-integrated chlorophyll, net primary production and stratification. Although stratification is increasing across the Indian Ocean, trends in chlorophyll and net primary production vary regionally, suggesting that increasing stratification will not necessarily result in reduced primary production in all parts of this basin.

1. Introduction

The Indian Ocean has experienced rapid basin-wide sea surface temperature (SST) warming due to climate change, with an average rise of 1°C between 1951 and 2015, and observations show that the Indian Ocean Warm Pool (IOWP), defined as water with SST values greater than 28°C, is significantly expanding (Roxy et al., 2020). Future climate projections suggest that the warming of the Indian Ocean will continue. Several studies have explored the effect of ocean warming on primary production in the Indian Ocean, but the impact of increased warming and stratification on productivity in this basin remains an open question. It has been widely hypothesized that climate change-induced ocean warming will result in a decrease in primary production due to increased stratification in the surface ocean (Richardson & Bendtsen, 2019). This increased stratification would result in a weakening of upward nutrient fluxes from depth, thereby reducing new production (Cermeño et al., 2008; Li et al., 2020). Changes in the stratification of the surface ocean can have significant impacts on phytoplankton growth and abundance. However, the effect of changes in stratification in driving trends in depth-integrated chlorophyll remains an unresolved question.

Validation: Marufa Ishaque
Visualization: Marufa Ishaque
Writing – original draft: Marufa Ishaque
Writing – review & editing: Marufa Ishaque, Sophie Clayton, John Klinck

Martinez et al. (2009) considered SST as an indicator of ocean stratification and based on ~20 years of satellite data (1980–2000) revealed that most parts of the Indian Ocean exhibited a parallel increase in surface chlorophyll and SST. By contrast, Dave and Lozier (2013) found that the strength of the correlation between stratification and surface chlorophyll in the Indian Ocean varied regionally, and overall found no strong correlation between these quantities. Additionally, they did not identify a significant time trend in chlorophyll in this region, but did find a decreasing trend in stratification across the low-latitude ocean due to faster warming of subsurface waters compared to the surface. Therefore, upper ocean warming does not always result in increased stratification. A combined data and model-based study (Roxy et al., 2016) found a decrease of up to 20% in phytoplankton biomass in the western Indian Ocean over the past six decades due to enhanced ocean stratification caused by surface warming. Similarly, a study using satellite data and Earth System Model solutions (Modi & Koll, 2023) found that in the tropical Indian Ocean, marine primary productivity decreased over the 1998–2022 period, particularly in the Arabian Sea (AS) and the coastal regions of the Bay of Bengal (BoB). Long-term remote sensing data from 1998 to 2015 were assimilated into an ocean biogeochemical model, which estimated a significant decline in annual primary production in the northern and Equatorial Indian Ocean; this decline is associated with the shoaling of the mixed layer and reduced nutrient inputs (Gregg & Rousseaux, 2019). Although warmer ocean temperatures can lead to a shallower mixed layer and increased light availability that initially promote phytoplankton growth (Gregg, 2005), phytoplankton can quickly deplete available nutrients in the well-illuminated mixed layer. As a result, surface abundance may decline while phytoplankton accumulate at greater depths, forming a layer of higher chlorophyll concentration that coincides with the nutricline (Somavilla et al., 2019). Although warming has occurred in the northern Indian Ocean, net primary production (NPP) has exhibited a significant increasing trend (2009–2019) in some parts of the basin (Kuttippurath et al., 2023), particularly in the western AS and the western BoB. Behrenfeld et al. (2006) found a reduction in NPP over most of the tropics due to increased stratification, but suggested an increase in NPP over the western Indian Ocean from 1998 to 2004. Using remote sensing data from 1998 to 2019, Dalpadado et al. (2021) found no significant trends of chlorophyll and NPP in most of the Indian Ocean. Sridevi et al. (2023) found a weak positive trend in NPP in the northern Indian Ocean and suggested that it was associated with an increase in the rate of nutrient deposition from atmospheric aerosols. Atmospheric deposition generally plays a minor role in the northern Indian Ocean (Singh et al., 2012). However, nitrogen deposition can offset the climate-driven decline in primary productivity trends in the central AS and the western BoB (Malsang et al., 2024). Overall, the differing results and conclusions from these studies show that there is currently no clear understanding of the relationship between stratification and depth-integrated chlorophyll and NPP, nor how they vary spatially in different parts of the Indian Ocean.

Most of the previous studies relating chlorophyll, primary production and stratification have either been conducted over a global domain (Behrenfeld et al., 2006; Dave & Lozier, 2013; Gregg, 2005; Martinez et al., 2009), or confined to a specific sub-basin of the Indian Ocean, such as the AS (Goes et al., 2005; Sun et al., 2023). Hammond et al. (2020) highlighted the importance of considering chlorophyll changes at a regional level. The BoB is characterized by low biological productivity compared to the AS, primarily due to weak vertical mixing and relatively weaker winds (Xu et al., 2021). Rainfall and river discharge freshen the upper BoB by 3–7 PSU, and SST can be 1.5–2°C warmer than in the central AS, contributing to strong stratification in the BoB (Prasanna Kumar et al., 2002). Stratification can inhibit surface chlorophyll concentrations but may enhance chlorophyll in the subsurface (Xu et al., 2021). By contrast, the AS is one of the most biologically productive regions in the world, driven by wind induced mixing, open ocean upwelling, and lateral advection, which supply nutrients to the euphotic zone (S. P. Kumar et al., 2009). Therefore, because of their geographical position and different physical and dynamical regimes, depth-integrated chlorophyll in these sub-basins of the northern Indian Ocean are expected to respond differently.

Two important climate modes affecting this region are the Indian Ocean Dipole (IOD) and El Niño Southern Oscillation (ENSO); both have a significant influence on ocean productivity because these climate modes impact on upwelling, vertical mixing, mixed layer depth and sea surface temperature (Pandey et al., 2019). ENSO is driven by ocean-atmosphere interactions in the tropical Pacific and consists of a cycle of warm El Niño and cold La Niña phases (McPhaden et al., 2006). Likewise, the IOD is driven by SST variability, where the western Indian Ocean alternately becomes warmer or cooler than the eastern basin, accompanied by corresponding changes in precipitation and wind patterns (N. H. Saji et al., 1999). Previous work has shown that observed chlorophyll concentrations in the Indian Ocean are impacted by both ENSO and IOD climate modes. Chlorophyll in the eastern EIO in fall and the southern BoB in winter are primarily related to IOD forcing, whereas ENSO has a

greater influence than IOD on chlorophyll in the Somalia upwelling region (Currie et al., 2013). In the eastern Arabian Sea, IOD and surface chlorophyll concentration is significantly and negatively correlated; therefore, during frequent positive IOD years, surface chlorophyll concentration is likely to decrease. However, during negative IOD due to increased Ekman suction and coastal upwelling, surface chlorophyll increases (Sankar et al., 2019). ENSO has a weaker influence on tropical thermocline variations than IOD and changes in this thermocline depth control the proximity of nutrient rich subsurface water to the euphotic zone and thus affect phytoplankton productivity (Currie et al., 2013). The influence of El Niño on chlorophyll anomalies is weaker compared with the influence of IOD over the northern Indian Ocean (Pandey et al., 2019). However, much of this previous work is based on satellite-derived surface chlorophyll concentrations, which do not consider how depth-integrated chlorophyll might be related to these climate modes and how this relationship varies regionally. In tropical and subtropical ocean regions, the bulk of chlorophyll is often found at depth in deep chlorophyll maxima (Cornec et al., 2021), which may not be well resolved by satellites. Therefore considering the full water column distribution of chlorophyll, not just surface distribution, will likely shed new light on the impact of climate modes such as IOD and ENSO on primary productivity in the Indian Ocean.

Phytoplankton play an important role in the biogeochemical cycles of many elements important to the global climate system, they are also responsible for half of the photosynthetic activity on earth (Field et al., 1998; Fox et al., 2020; McCluskey et al., 2022). Chlorophyll concentration is usually used as a proxy for phytoplankton abundance (McCluskey et al., 2022). The growth rate and abundance of phytoplankton, and the concentration of chlorophyll, are largely controlled by the availability of nutrients (e.g., nitrate, phosphate), water temperature and light (Li et al., 2020). These phytoplankton growth limiting factors are regulated by a wide range of physical processes, for example, mixed-layer dynamics, ocean circulation, upwelling, solar cycle, atmospheric dust deposition (Behrenfeld et al., 2006). Only about 25% of global primary production occurs in the upper 10 m, and subsurface primary production increases in regions with a deeper nutricline (Bendtsen et al., 2023). At latitudes where solar radiation is abundant, such as in the tropical and subtropical Indian Ocean, the production of new biomass is primarily determined by the vertical supply of nutrients into the euphotic zone (Falkowski et al., 1998). In tropical regions like the Indian Ocean, chlorophyll concentrations are typically higher below the mixed layer, near the base of the euphotic zone, usually between 50 and 200 m; the depth at which this chlorophyll maximum occurs is referred to as the deep chlorophyll maximum (DCM) (Mignot et al., 2014). The DCM occurs at the depth where optimal levels of light and nutrients coincide (Jayaram et al., 2021). Therefore, in subtropical and tropical oceans, surface chlorophyll concentrations are often not representative of the overall phytoplankton abundance of the water column.

Though several previous studies have used remote-sensing, modeling and/or sparse in situ chlorophyll data largely from the surface ocean (Martinez et al., 2009; Roxy et al., 2016; Sridevi et al., 2023), a lack of depth-resolved sub-surface chlorophyll data collected over several years has limited the scope of that previous work. Chlorophyll concentrated at the base of the Mixed Layer Depth (MLD) is invisible to satellites, often reflecting nutrient depletion in the overlying waters (Strutton et al., 2023). Traditional approaches using ships and moorings require expensive instrumentation and not all areas of the Indian Ocean are accessible. These have limitations in terms of temporal, horizontal, and vertical measurement resolution. Satellites can provide productivity estimations with enhanced space-time coverage but have limitations in terms of accuracy of satellite ocean color observations and are not capable of detecting subsurface information where chlorophyll may still be significant (Izett et al., 2023). Thanks to the deployment of Biogeochemical-Argo (BGC-Argo) floats, that are equipped with biogeochemical sensors (Bittig et al., 2019), in situ subsurface measurements of biogeochemical variables over a range of temporal and spatial scales are now becoming available for many historically under-sampled ocean regions, including the Indian Ocean. Data from BGC-Argo floats have been used in a small number of studies of biogeochemical processes in the Indian Ocean, such as along-track chlorophyll variability (Jayaram et al., 2021), chlorophyll responses to the passage of a cyclone (Jayaram et al., 2019), inter-annual and intra-seasonal variability of dissolved oxygen (Prakash et al., 2012), and the depth-distribution of chlorophyll and particulate organic carbon in mesoscale eddies (Strutton et al., 2023). However, this wealth of depth-resolved chlorophyll data from the Indian Ocean has so far been underutilized because much of it, although available, has not been fully quality controlled. In the work presented here, we use all available BGC-Argo chlorophyll data from 2013 to 2022 to examine the relationship between stratification and chlorophyll, how trends in these quantities have changed over time, and how climate modes such as ENSO and IOD play a role in modulating the observed trends in the northern and the Equatorial Indian Ocean.

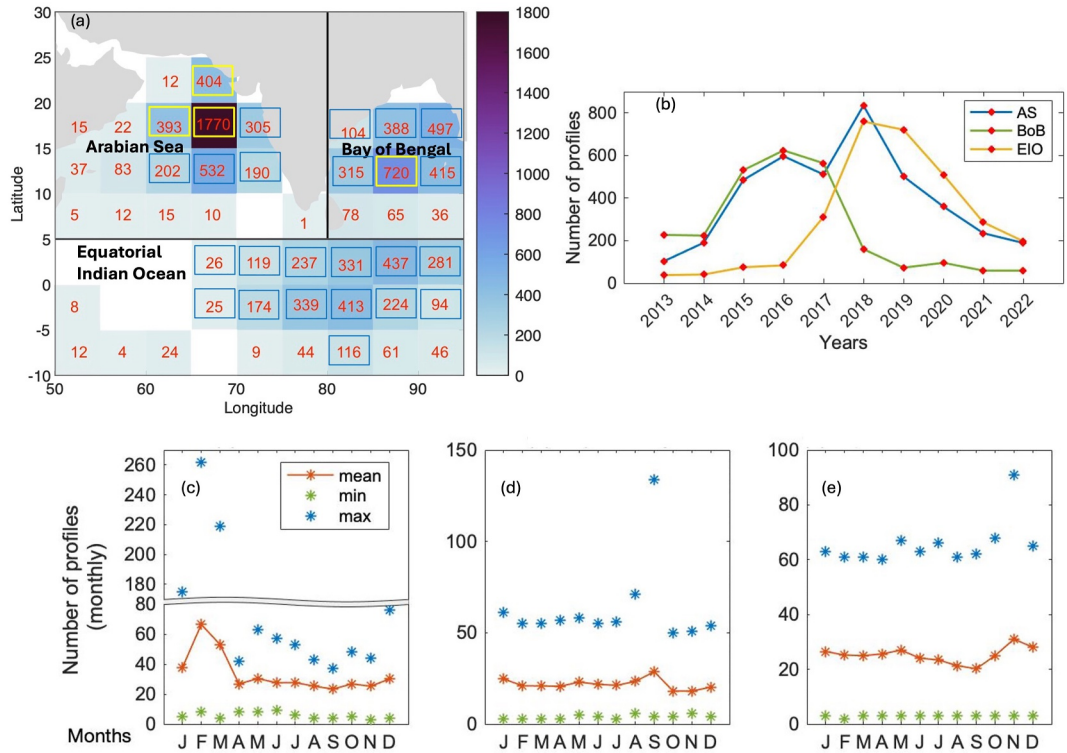

Figure 1. Spatial and temporal distribution of BGC-Argo profiles used in this study: (a) the profile count within each 5° by 5° spatial bin and within each of the study sub-regions: Arabian Sea (AS), Bay of Bengal (BoB) and Equatorial Indian Ocean (EIO) delineated by thick black lines, the blue outlines around the profile counts indicate the bins which have minimum 5 years of data, and the yellow outlines indicate the bins which have a full 10 years of data, (b) the yearly distribution of total number of profiles for each of the sub-regions, (c) mean (orange), maximum (blue) and minimum (green) number of profiles per month within the (c) Arabian Sea, (d) Bay of Bengal and (e) Equatorial Indian Ocean.

2. Data and Methods

2.1. Study Region and Study Period

Our study region encompasses the northern and Equatorial Indian Ocean, which we have defined as extending from 10°S to 25°N and 50°E to 95°E, and can be further subdivided into sub-regions defined as follows: the Arabian Sea (AS), 5°N to 25°N and 50°E to 80°E; the Bay of Bengal (BoB), 5°N to 25°N and 80°E to 95°E; and the Equatorial Indian Ocean (EIO), 10°S to 5°N and 50°E to 95°E (Figure 1a). Seasonality in this region is dominated by the South Asian Monsoon, an important driver of physical and biogeochemical processes, and one can broadly define the summer monsoon as occurring during June through September, and the winter monsoon as occurring during November through February. The duration of the study period was constrained by the availability of BGC-Argo float data, and spans from January 2013 to December 2022 (Figure 1; Figures S1 and S2 in Supporting Information S1), as very few profiles were available for 2012 when the initial float deployments took place.

2.2. BGC-Argo Data

BGC-Argo floats are equipped with sensors that measure dissolved oxygen, pH, dissolved nitrate, downwelling irradiance, chlorophyll fluorescence, and particulate back-scattering coefficient (Bittig et al., 2019) along with temperature, salinity, and pressure. However, not all BGC-Argo floats are equipped with all of these sensors. For this study, we used only float data where both chlorophyll fluorescence and particulate backscattering coefficient (bbp) were measured, as both of these parameters are needed to estimate net primary production (NPP) from the float profiles.

BGC-Argo data collected within the study region and used for this study were accessed on 20 February 2023 (https://argo.ucsd.edu/data/). We downloaded and used synthetic profile (Sprof) files, which contain all the profile data for a single float in NetCDF format and provide all of the physical and biogeochemical variable data along a common pressure axis. For the study period (2013–2022), there were 10,756 vertical profiles from 58 floats within our study region which measured chlorophyll, bbp, temperature, salinity, and pressure (Figure 1). After applying quality control (QC) checks to the data (described fully in Section 2.3, below), around 10% of the profiles were discarded due to data quality issues, we retained a total of 9,650 profiles for further analysis. Depth resolution was not consistent across all the profiles in our reduced QC'd data set, so all of the profile data were linearly interpolated onto a common regular 1 m depth grid from 1 to 1000 m. All data were checked visually to detect any drift over time which could indicate sensor drift.

2.3. Quality Control and Adjustment of BGC-Argo Chlorophyll and bbp Data

BGC-Argo floats are equipped with WETLABS/Sea-bird Scientific (SBE) fluorometer sensors (fluorometer with excitation and emission at 470 and 695 nm) to collect fluorescence data. Chlorophyll-a concentrations (Chl) are obtained from raw fluorescence data, following the manufacturer's instructions, by using the equation:

$$Chl = (fluorescenceChl - darkChl) \times scaleChl \quad (1)$$

where $fluorescenceChl$ is the chlorophyll-a signal obtained from fluorescence, $scaleChl$ is the slope of the calibration equation, and $darkChl$ is the dark value or the measurements taken in the absence of light; $scaleChl$ and $darkChl$ are both provided by the manufacturer (Schmechtig et al., 2018). In this paper, we use the term "chlorophyll" to refer to chlorophyll-a throughout. We quality controlled all of the float chlorophyll data following recommended BGC-Argo quality control procedures (Schmechtig et al., 2018). Raw chlorophyll data were corrected to account for common factors that impact data quality including, but not limited to, biofouling, instrument drift, and sensor failures. The quality control process includes the exclusion of bad data, dark correction (removing the median of the minimum chlorophyll from raw chlorophyll values), global range test (excluding data outside the range of $0 - 50$ mg m^{-3}), and a correction for non-photochemical quenching (NPQ). NPQ occurs when phytoplankton are exposed to high irradiance, resulting in a decrease in fluorescence (Cullen & Lewis, 1995; Su et al., 2021) which can result in falsely identifying a deep chlorophyll maximum (DCM) in profiles impacted by NPQ. If the maximum chlorophyll observed in a profile is within the upper 90% of the mixed layer, it is assumed to be due to NPQ, and that maximum value is then extrapolated to the surface (Xing et al., 2012). The chlorophyll data were further divided by 2, to account for previously identified biases in conversion from in situ fluorescence to chlorophyll (Roesler et al., 2017).

2.4. NPP Estimation

Net Primary Production (NPP) is defined as gross photosynthetic carbon fixation minus the organic carbon respired by phytoplankton communities (Yang et al., 2022). To estimate NPP in this study, we applied the carbon-based productivity model (CbPM; Yang et al. (2022); Westberry et al. (2008); Behrenfeld et al. (2005)) to the float data. CbPM has been shown to produce a good agreement between NPP estimated from float data and NPP estimated from ^{14}C incubations (Yang et al., 2021).

We used bbp data from the floats, which were quality controlled according to recommended BGC-Argo quality control procedures (Dall'Olmo et al., 2019), including the following tests: missing data, high deep value, negative bbp, and noisy profiles. For each profile, the missing data test was performed by dividing the upper 1,000 dbar into 10 pressure bins; the threshold for a minimum number of data per bin was defined as 1. The high deep value test was performed to detect any anomalously high bbp values deeper than 700 dbar, and the high deep value threshold was set at 0.0005 m^{-1}. A negative bbp test was performed for each profile and any negative bbp values were removed. To remove noisy data, a noisy profile test was applied to the profiles which had at least 10 data points. Absolute residuals were computed between bbp and median-filtered bbp, and if the absolute residual was below 0.0005 m^{-1}, the data were retained and used in our analyses.

In this paper, we followed the method described in Yang et al. (2022) to calculate NPP (mg C m^{-3} day^{-1}) using Equation 2, the product of phytoplankton carbon (C_{phyto}, mg C m^{-3}) and phytoplankton specific growth rate (μ, day^{-1}):

$$NPP = C_{phyto} \times \mu \quad (2)$$

We calculated C_{phyto} from bbp at 470 nm (bbp_{470}) using the empirical relationship derived by Graff et al. (2015), and given below in Equation 3. Since the floats measured bbp at 700 nm (bbp_{700}, m^{-1}), we first converted it to bbp_{470} (m^{-1}) using Equation 4 and the relationship derived by Boss et al. (2013).

$$C_{phyto} = 12128 \times bbp_{470} + 0.59 \quad (3)$$

$$bbp_{470} = bbp_{700} \times \left(\frac{470}{700}\right)^{-0.78} \quad (4)$$

The phytoplankton specific growth rate, μ, was estimated based on the method described in Westberry et al. (2008) using Equation 5, where *Chl* is the float-measured chlorophyll concentration (mg m^{-3}) and I_z is the daily mean light level at each depth (mol photons m^{-2} day^{-1}). Using Equation 6, I_z was estimated from photosynthetically active radiation (PAR) at the ocean surface (PAR_{surf}), depth (Z), and diffuse attenuation coefficient of PAR (K_{PAR}).

$$\mu = \frac{2 \times Chl/C_{phyto} \times \left(1 - e^{-5I_z}\right)}{0.022 + (0.045 - 0.022) \times e^{-3I_z}} \quad (5)$$

Surface PAR was obtained from monthly 0.167° by 0.167° Moderate Resolution Imaging Spectroradiometer (MODIS) data (Yang et al., 2022) (https://oceancolor.gsfc.nasa.gov). The time and location of each BGC-Argo profile were matched with the nearest surface PAR estimate using the MATLAB knnsearch function which uses the k-nearest neighbor algorithm and only those which matched surface PAR values were extracted and used.

$$I_z = PAR_{surf} \times \exp(-K_{PAR} \times Z) \quad (6)$$

The mixed layer depth (MLD) was calculated based on the density threshold criteria 0.03 kg m^{-3} by considering reference density at 10 dbar (De Boyer Montégut et al., 2004). When MLD $\leq K_{490}^{-1}$, Equation 7 was used to calculate K_{PAR} (m^{-1}) and when MLD $> K_{490}^{-1}$, Equation 8 was used to calculate K_{PAR} (Morel et al., 2007; Yang et al., 2022).

$$K_{PAR} = 0.0864 + 0.884 \times K_{490} - 0.00137 \times K_{490}^{-1} \quad (7)$$

$$K_{PAR} = 0.0665 + 0.874 \times K_{490} - 0.00121 \times K_{490}^{-1} \quad (8)$$

To calculate K_{PAR}, we used the float-measured chlorophyll-a concentration (Chl) to estimate K_{490} in Equation 9, the 490 nm diffuse attenuation coefficient (m^{-1}):

$$K_{490} = 0.0166 + 0.07242 \times Chl^{0.68955} \quad (9)$$

The euphotic zone (depth to which 1% of surface PAR remains) in our study region is generally no deeper than 150 m (Siegel et al., 2014; Stramska & Cieszyńska, 2015) and using in situ measurements during April–May 2014, Dalabehara and Sarma (2021) found that the euphotic depth varied between 41 and 135 m in the Indian Ocean. To include all the available chlorophyll found at or below the 1% irradiance depth (Hanson et al., 2007), depth-integrated chlorophyll and depth-integrated NPP were estimated to 200 m depth.

The DCM depth was identified as the depth where the maximum chlorophyll concentration was observed (Barbieux et al., 2019; Jayaram et al., 2021). To identify the DCM in our study, we assumed that no living phytoplankton were found below 200 m, and identified the depth of maximum chlorophyll concentration from the interpolated profiles; if the identified maximum chlorophyll value was greater than twice the median of the chlorophyll values in the first 15 m, then that was considered the DCM (Cornec et al., 2021). If the DCM is below the MLD, then it can represent either a Deep Biomass Maximum (DBM) or a Deep photoAcclimation Maximum

(DAM). A DBM represents a true maximum in phytoplankton biomass in terms of carbon, whereas a DAM results from phytoplankton photoacclimation, where phytoplankton increase their cellular chlorophyll to carbon biomass ratio as a response to low irradiance levels (Masuda et al., 2021). A global assessment of DCMs using chlorophyll and bbp data from BGC-Argo profiles found that the northern part of the Indian Ocean the DCM generally represents a DBM rather than a DAM (Cornec et al., 2021), therefore, a better understanding of depth-resolved phytoplankton abundance can help quantify carbon budgets in this region. The mean chlorophyll (or NPP) from the top 10 m depth is considered the surface chlorophyll (or surface NPP).

2.5. Calculation of Physical Oceanographic Parameters

BGC-Argo temperature and salinity data were converted to conservative temperature and absolute salinity, respectively, to obtain potential density. BGC-Argo float data include water pressure rather than depth, so water depth in meters was calculated from the pressure and location data. The vertical stratification was estimated from the Brunt–Väisälä or buoyancy frequency (N^2). The maximum value was the maximum N^2 and the corresponding depth was considered as the depth of maximum N^2. All conversions and computations of derived physical properties were done using the MATLAB Gibbs-SeaWater (GSW) Oceanographic Toolbox (https://www.teos-10.org/) (Li et al., 2020).

2.6. Climate Modes: ENSO and IOD

Two climate modes were considered as part of this study: the IOD and ENSO. The IOD can be represented by the Dipole Mode Index (DMI) which uses the SST gradient between the western EIO (50°E–70°E and 10°S–10°N) and the southeastern EIO (90°E–110°E and 10°S–0°N). Positive (negative) values of the DMI refer to positive (negative) IOD modes (N. H. Saji et al., 1999). Monthly DMI data was downloaded from the NOAA Physical Science Laboratory website https://psl.noaa.gov/data/timeseries/month/DMI/ (N. Saji & Yamagata, 2003).

Multivariate ENSO Index Version 2 (MEI.v2) was used to represent ENSO (Wolter & Timlin, 2011; Zhang et al., 2019). This bimonthly index is the time series of a combined Empirical Orthogonal Function (EOF) of five different variables: sea level pressure, SST, zonal and meridional surface wind components and outgoing longwave radiation over the tropical Pacific basin (30°S–30°N and 100°E–70°W). It was downloaded from https://psl.noaa.gov/enso/mei/.

2.7. Statistical Analyses

In order to balance the need to retain spatial information, but also pool sufficient points in time to identify temporal trends in the data, we binned the BGC-Argo profiles spatially into 5° by 5° bins. Spatial bins which contained fewer than 20 profiles were excluded from the analyses as statistical tests showed that fewer than 20 profiles did not produce significant results. Statistical significance was defined as a probability value (p-value) less than or equal to the significance level, which was 0.05 (5%). Monthly mean values and standard deviations were calculated for each month for years 2013–2022 for depth-integrated chlorophyll, depth-integrated NPP, DCM, MLD, surface NPP, surface chlorophyll, maximum N^2, and the depth of maximum N^2. These monthly mean values were then interpolated in time to produce a mean interpolated daily climatological product to avoid sharp jumps in data values from month to month when calculating anomalies. Anomalies of depth-integrated chlorophyll, surface chlorophyll, DCM, depth-integrated NPP, surface NPP, MLD, maximum N^2, and the depth of maximum N^2 were calculated by subtracting the daily interpolated climatology data (on the corresponding yearday) from the observed profile data (collected on a particular yearday). The anomaly data were used in the calculation of trends and correlations.

We tested each of the variables to assess whether they were normally distributed using the Kolmogorov-Smirnoff test. We found that the variables used to calculate trends were not normally distributed, and so we applied the Mann-Kendall test and Sen's method to each 5° by 5° spatial bin for each dependent variable separately: the depth-integrated chlorophyll anomaly, buoyancy frequency anomaly, depth-integrated NPP anomaly and MLD anomaly. The Mann-Kendall test is a non-parametric test used to determine the presence of trends (which may or may not be linear) in the data, and Sen's method calculates the magnitude of those trends. Sen's slope was used to calculate the percent change per year by dividing the slope by the mean value of the variable within each spatial bin. The trends were calculated at the 95% confidence level. The independent variable for this trend analysis was

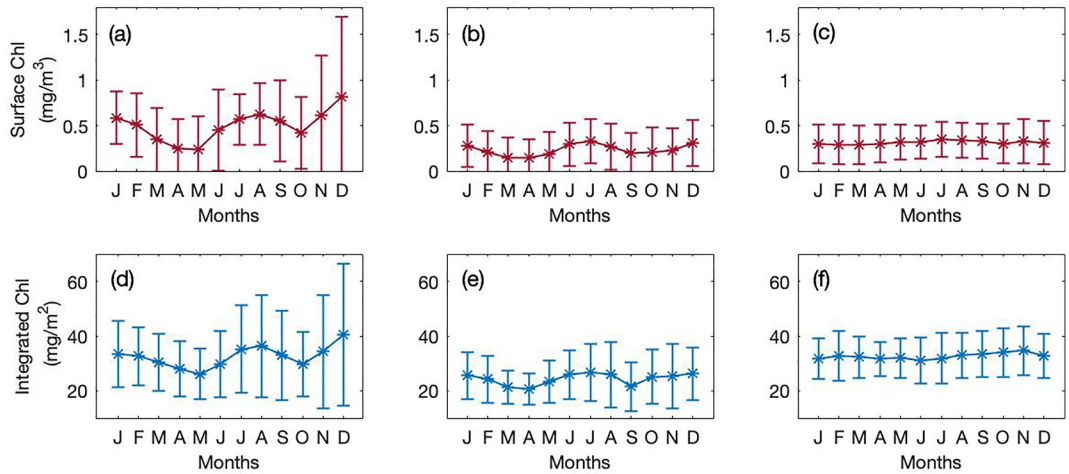

Figure 2. Monthly mean surface chlorophyll (mg m^{-3}) with standard deviation (a) Arabian Sea, (b) Bay of Bengal, and (c) Equatorial Indian Ocean and depth-integrated chlorophyll (mg m^{-2}) with standard deviation (d) Arabian Sea, (e) Bay of Bengal, and (f) Equatorial Indian Ocean.

time, and within each 5° by 5° spatial bin, the dates of all the available profiles are discrete. Not all spatial bins had data coverage for the entire 10 year period (Table S1; Figure S3 in Supporting Information S1). Therefore, for each spatial bin, we considered the span between the first and last years of observation, including any gaps within this interval, when discussing our results. This basin-wide trend analysis allowed us to identify regions that have either significant positive or negative trends.

Three spatial bins were selected, one each from the AS, BoB, and the EIO, where the maximum positive stratification trends were observed. The objective was to assess whether the observed increase in stratification was primarily driven by changes in salinity or temperature. To perform this analysis, the thermal expansion coefficient (alpha) and the haline contraction coefficient (beta) were calculated. Temperature and salinity gradients were then computed between 15 and 150 m depths. The product of alpha and the temperature gradient represented the thermal contribution to stratification, while the product of beta and the salinity gradient represented the haline contribution. The ratio of thermal to haline contributions was calculated for each of those spatial bins across all available years. A ratio greater than 1 indicates that thermal effects dominate over salinity effects. Finally, the first and last years of a specific month were compared to evaluate temporal changes in stratification drivers.

Since the variables that were used to conduct the correlation analyses were not normally distributed, Spearman's rank correlation was performed at 95% confidence. Correlations were conducted using the maximum N^2, depth of max-N^2, MLD, and DCM anomalies against depth-integrated chlorophyll and depth-integrated NPP anomalies. For each spatial bin, all of the available data were used to perform correlations between the anomalies of all variables. These correlations indicate how the variables are related and identify spatial bins where significant correlations exist. To understand the correlation between the ENSO and IOD climate modes and depth-integrated chlorophyll, Spearman's rank correlation was conducted between the IOD or ENSO index and depth-integrated chlorophyll and depth-integrated NPP anomalies. All of the statistical analyses described here were implemented using MATLAB.

3. Results

3.1. Monthly Variability in Chlorophyll, NPP, Stratification, DCM, and MLD

Surface and depth-integrated chlorophyll were consistently higher on average in the AS than the BoB and the EIO (Figure 2). In the AS, surface and depth-integrated chlorophyll concentrations exhibited a semi-annual pattern with peaks in August and December (Table 1). Lower surface and depth-integrated chlorophyll concentrations were observed in May and October. We also observed a semi-annual pattern in the BoB, but it was less pronounced than in the AS (Figure 2) with both surface and depth-integrated chlorophyll concentrations lower in April and September and higher in July and December. We observed the least seasonal variation in chlorophyll

Table 1
Mean Seasonal Highest and Lowest Values of Surface Chlorophyll (surfChl; mg m^{-3}), Depth-Integrated Chlorophyll (intChl; mg m^{-2}), Surface NPP (surfNPP; mg m^{-3} day^{-1}) and Depth-Integrated NPP (intNPP; mg m^{-2} day^{-1}) for the Arabian Sea (AS), Bay of Bengal (BoB) and Equatorial Indian Ocean (EIO) Sub-Regions

	AS	BoB	EIO
surfChl (mg m^{-3})			
Highest	August, December	July, December	July
	0.62 ± 0.34, 0.82 ± 0.88	0.33 ± 0.24, 0.31 ± 0.25	0.35 ± 0.20
Lowest	May, October	April, September	March
	0.24 ± 0.36, 0.42 ± 0.40	0.14 ± 21, 0.20 ± 0.23	0.29 ± 0.21
intChl (mg m^{-2})			
Highest	August, December	July, December	November
	36 ± 19, 41 ± 26	28 ± 11, 26 ± 10	34 ± 9
Lowest	May, October	April, September	June
	26 ± 9, 30 ± 12	21 ± 6, 22 ± 9	31 ± 8
surfNPP (mg C m^{-3})			
Highest	August, December	July, December	July
	51 ± 31, 74 ± 82	30 ± 22, 28 ± 23	31 ± 17
Lowest	May, October	April, September	March
	22 ± 33, 38 ± 36	13 ± 19, 18 ± 21	26 ± 19
intNPP (mg C m^{-2})			
Highest	August, December	July, December	August
	2367 ± 862, 2566 ± 1334	1407 ± 734, 1484 ± 835	1462 ± 626
Lowest	May, October	April, September	March
	874 ± 627, 1741 ± 946	520 ± 335, 978 ± 641	978 ± 534

Note. For each case, the month of the year corresponding to the highest/lowest concentrations is indicated. The ± values represent the standard deviation.

concentrations in the EIO, where the lowest mean monthly depth-integrated chlorophyll was seen in June and a slightly higher value observed during November. Overall, depth-integrated chlorophyll in the EIO was slightly higher than in the BoB, but lower than in the AS.

In the AS, surface and depth-integrated NPP both exhibited a semi-annual pattern (Figure 3) with peaks in August and December, and lower values observed in May and October (Table 1). The BoB also exhibited a semi-annual pattern, though it was not as prominent as in the AS, with both surface and depth-integrated NPP being lower during April and September and higher during July and December. Depth-integrated NPP in the EIO had the lowest values in March and slightly higher values from August to November. Surface NPP in the EIO did not show any marked seasonal patterns, and the highest surface NPP was observed in July and the lowest surface NPP observed in March.

In the AS and the BoB, the MLD had a semi-annual pattern (Figure 4): shallower during April and October, and deeper in July and January (Table 2). In the EIO, the MLD followed an annual pattern and was shallower in December and deeper in August. The depth of the DCM followed a semi-annual pattern in the AS, and an annual pattern in the BoB and EIO (Figure 4). In the AS, the DCM was deepest in May and shallowest in September. Similarly, in the BoB, the DCM was deepest in May and shallowest in November. In the EIO, the shallowest and deepest DCMs were observed in December and July, respectively (Table 2). Our results also show that in December/January and July/August the MLD and DCM coincided in the AS. Though the DCM and MLD converged in July/August in all three basins, they only converged fully in the AS. The DCM and MLD were found to occur at significantly different depths in each basin of the study region during April and May.

The EIO was most strongly stratified, with higher maximum N^2 than the AS and the BoB (Figure 5). Maximum N^2 was found to be slightly weaker in May in the EIO. In the AS, the strength of stratification was highest in July,

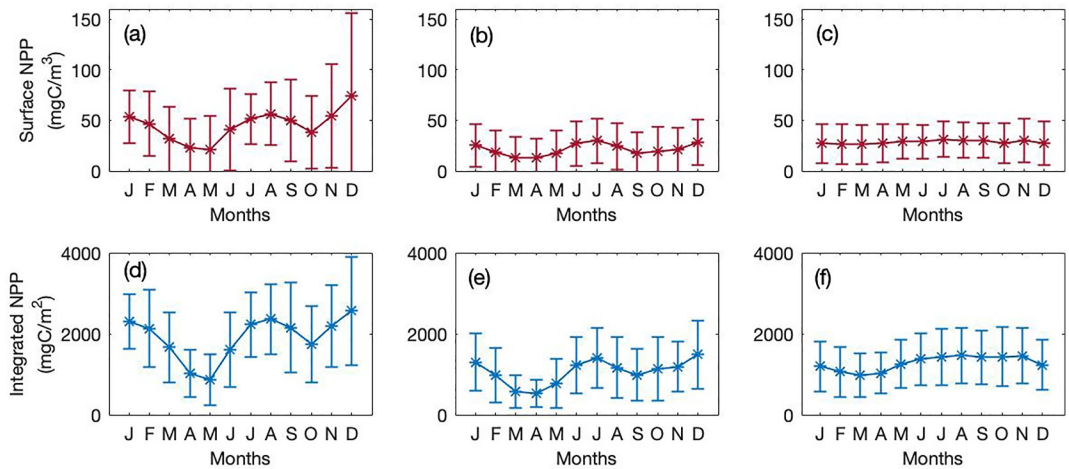

Figure 3. Monthly mean surface net primary production (mg C m^{-3}) with standard deviation (a) Arabian Sea, (b) Bay of Bengal, and (c) Equatorial Indian Ocean and depth-integrated net primary production (mg C m^{-2}) with standard deviation (d) Arabian Sea, (e) Bay of Bengal, and (f) Equatorial Indian Ocean.

and was lowest in March (Table 2). The BoB had the strongest stratification from August to October compared with weaker stratification in March. The depth of maximum N^2 showed a semi-annual pattern in the AS and the EIO and an annual pattern in the BoB (Figure 5). During March–June, the AS had the shallower depths of maximum N^2 with the shallowest in May. However, during those months, the BoB had deeper depths of maximum N^2, with the deepest in April. The deepest maximum N^2 in the AS was in August (Table 2). Both AS and BoB had shallower maximum N^2 in October. The depths of maximum N^2 in the EIO from June to January were deeper than the AS and the BoB. The deepest maximum N^2 in the EIO were observed in July and the shallowest in April.

3.2. Temporal Trends in Depth-Integrated Chlorophyll, NPP, Stratification, and Mixed Layer Depth

The temporal trends in depth-integrated chlorophyll are shown in Figure 6a. Out of the 36 5° by 5° spatial bins that contained data, significant trends were identified in 19 bins, of which eight had negative, and 11 had positive trends. Regionally, the BoB had a generally positive trend in depth-integrated chlorophyll: five out of six bins had significant positive trends. All these spatial bins contained at least five years of data, with one bin (10°N to 15°N, 85°E to 90°E) containing 10 years of observations (bin number 17). The maximum trend value observed was 4.1 mg $m^{-2}yr^{-1}$ chlorophyll in the western BoB, while the minimum trend value was 1 mg $m^{-2}yr^{-1}$. One spatial bin in the central northern BoB had a significant negative trend in depth-integrated chlorophyll (−1.2 mg $m^{-2}yr^{-1}$); this bin contained 7 years of data (bin number 9) from 2013 to 2019 (Table S1 in Supporting Information S1). In the AS, four spatial bins on the eastern side of the basin showed significant negative trends with a

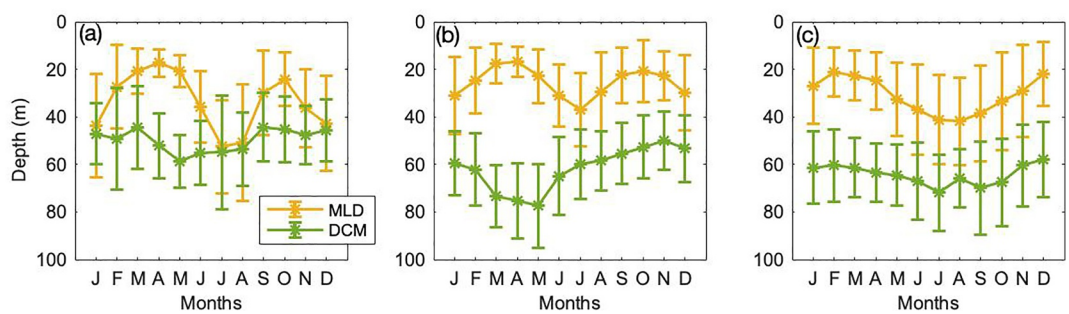

Figure 4. Monthly mean Mixed Layer Depth (MLD; m) and Deep Chlorophyll Maximum (DCM; m) of (a) Arabian Sea, (b) Bay of Bengal, and (c) Equatorial Indian Ocean with standard deviation. Note that the *y*-axis has been inverted so that the ocean surface is represented by the upper limit of the axis.

Table 2
Mean Seasonal Highest and Lowest Values of Mixed Layer Depth (MLD; m), Depth Chlorophyll Maxima (DCM; m), Maximum Stratification (Max N^2; s^{-2}) and the Depth of Maximum Stratification (Max N^2 Depth; m) for the Arabian Sea (AS), Bay of Bengal (BoB) and Equatorial Indian Ocean (EIO) Sub-Regions

	AS	BoB	EIO
MLD (m)			
Deepest	July, January	July, January	August
	52 ± 19, 44 ± 22	37 ± 15, 31 ± 16	42 ± 18
Shallowest	April, October	April, October	December
	17 ± 6, 24 ± 11,	17 ± 6, 21 ± 13	22 ± 14
DCM (m)			
Deepest	May	May	July
	59 ± 11	77 ± 18	72 ± 16
Shallowest	September	November	December
	44 ± 14	50 ± 12	58 ± 16
Max N^2 (s^{-2})			
Highest	July	August	January
	0.0015 ± 0.00082	0.0022 ± 0.0012	0.0029 ± 0.002
Lowest	March	March	May
	0.00071 ± 0.00051	0.0012 ± 0.0047	0.0024 ± 0.0012
Max N^2 depth (m)			
Deepest	August	April	July
	77 ± 28	84 ± 44	89 ± 25
Shallowest	May	September	April
	33±20	45 ± 28	66 ± 24

Note. For each case, the month of the year corresponding to the highest/lowest concentrations is indicated. The ± values represent the standard deviation.

largest of −1.7 mg $m^{-2}yr^{-1}$ and smallest of −1 mg $m^{-2}yr^{-1}$. Among these four bins, two contained (bin numbers 2 and 6) 10 years of data (15°N to 25°N, 65°E to 70°E), while the remaining two bins contained nine (bin number 14) and 7 years (bin number 7) of data. Conversely, two spatial bins on the western side of the AS showed significant positive trends with a maximum of 3 mg $m^{-2}yr^{-1}$ and minimum of 1.8 mg $m^{-2}yr^{-1}$ depth-integrated chlorophyll (Figure 6a). One of these two bins (bin number 5) had 10 years of data (15°N to 20°N, 60°E to 65°E). These two bins were also flanked to the south by two bins where the trends were positive, but not statistically significant. In the EIO, four spatial bins showed significant positive trends in depth-integrated chlorophyll, which contained 5 (bin number 45), 6 (bin number 28), 7 (bin number 29), and 9 years (bin number 36) of data (Figure S3; Table S1 in Supporting Information S1). In contrast, three spatial bins showed significant negative trends, two of which contained eight (bin numbers 32 and 37) years of data. The maximum increasing trend (within four spatial bins) in the EIO was 2 mg $m^{-2}yr^{-1}$ and minimum was 0.8 mg $m^{-2}yr^{-1}$ and the largest decreasing trend (within three spatial bins) was −9.7 mg $m^{-2}yr^{-1}$ and weakest was −0.8 mg $m^{-2}yr^{-1}$ chlorophyll.

The temporal trends in depth-integrated NPP revealed that only 12 spatial bins (out of 36) had significant trends, eight bins showed significant positive trends, and four showed significant negative trends (Figure 6b). The AS had both increasing (two spatial bins; maximum of 227 mg C $m^{-2}yr^{-1}$ and minimum 181 mg C $m^{-2}yr^{-1}$) and decreasing (two spatial bins; maximum of −110 mg C $m^{-2}yr^{-1}$ and minimum −107 mg C $m^{-2}yr^{-1}$) trends. These were split zonally, with increasing and decreasing integrated NPP trends found on the western and eastern AS, respectively. Both spatial bins with decreasing trends had 10 years of data (bin numbers 2 and 6). The bin showing an increasing trend (15°N to 20°N, 60°E to 65°E) also had 10 years of data (Figure S3 in Supporting Information S1). The BoB, however, had an almost consistently positive trend in integrated NPP, with four bins exhibiting significant positive trends (maximum of 426 mg C $m^{-2}yr^{-1}$ and minimum 88 mg C $m^{-2}yr^{-1}$). Among all these bins, only one bin (10°N to 15°N, 85°E to 90°E) had 10 years of data (bin number 17), while the remaining bins had at least five years of data. In the EIO, two spatial bins had positive trends (maximum value was 80 mg C $m^{-2}yr^{-1}$ and minimum 64 mg C $m^{-2}yr^{-1}$) and two spatial bins had negative trends in depth-integrated NPP (largest value

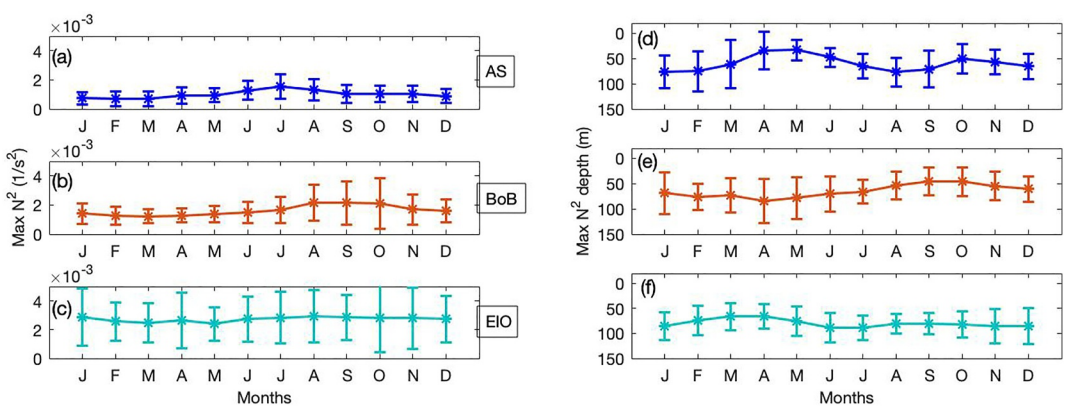

Figure 5. Monthly mean maximum buoyancy frequency N^2 (s^{-2}) of (a) Arabian Sea, (b) Bay of Bengal, (c) Equatorial Indian Ocean, and the depth of maximum buoyancy frequency (m) of (d) Arabian Sea, (e) Bay of Bengal, (f) Equatorial Indian Ocean. Note that the *y*-axis has been inverted so that the ocean surface is represented by the upper limit of the axis.

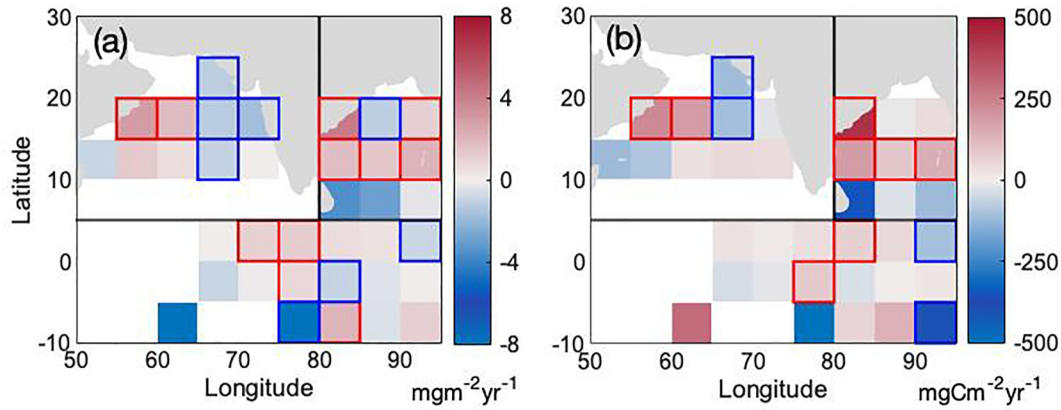

Figure 6. Time trends of (a) depth-integrated chlorophyll (IntChl, mg $m^{-2}yr^{-1}$) anomaly and (b) depth-integrated NPP (IntNPP, mg C $m^{-2}yr^{-1}$) anomaly with $p \leq 0.05$ significance. Spatial bins with red/blue borders indicate significant positive/negative trends. The black lines separate regions of Arabian Sea, Bay of Bengal, and Equatorial Indian Ocean.

of −404 mg C $m^{-2}yr^{-1}$ and smallest value of −104 mg C $m^{-2}yr^{-1}$). Spatial bins showing positive trends in the EIO contained eight to 9 years of data, while one of the bins showing a negative trend contained 8 years of data (Table S1 in Supporting Information S1). The highest maximum positive trends in depth-integrated NPP were observed in the BoB.

The temporal trends in maximum stratification (max N^2) were significantly positive in most parts of the study region, 17 bins showed significant positive trends out of a total of 36, and only three had significant negative trends overall (Figure 7a). In the BoB, six spatial bins in the northern part of the basin showed significant positive trends (maximum positive trend of 3.1× 10^{-4} $s^{-2}year^{-1}$ and minimum of 7.8× 10^{-5} $s^{-2}year^{-1}$). Among these, only one spatial bin (bin number 17) had 10 years of data, while the remaining bins had at least 5 years of data (Figure S3 in Supporting Information S1). We have bins with similar length of time series on both sides of the BoB. Only one spatial bin in the southern part of the BoB had a significant negative trend (−2.6× 10^{-4} $s^{-2}year^{-1}$), and this bin contained 4 years of data (bin number 25). Although it was flanked by two adjacent bins that also showed negative trends, those trends were not statistically significant in max N^2. These results also suggested that stratification is increasing more on the western side of the BoB than on the eastern side, with the highest positive trend values for max N^2 observed off the eastern coast of the Indian subcontinent. In the AS, four bins exhibited significant positive trends in max N^2, with the maximum trend value of 5.9× 10^{-5} $s^{-2}year^{-1}$ and the minimum trend value of 3.8× 10^{-5} $s^{-2}year^{-1}$. Three of these spatial bins (bin numbers 2, 5, 6) had 10 years of data (Figure

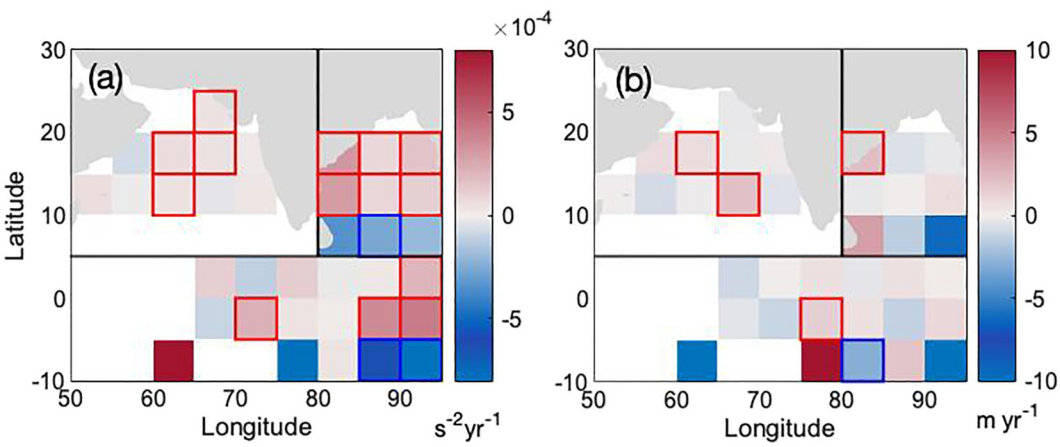

Figure 7. Time trends of (a) maximum stratification (Max N^2, $s^{-2}yr^{-1}$) anomaly and (b) mixed layer depth (MLD, m yr^{-1}) anomaly with $p \leq 0.05$ significance. The spatial bins with red/blue borders indicate significant positive/negative trends. The black lines separate three regions of Arabian Sea, Bay of Bengal, and Equatorial Indian Ocean.

Table 3
Correlation Coefficients (Strongest Positive/Negative Values Only Over the Significant Spatial Bins, Within a Region) of the Anomalies of Stratification Strength (Max N^2), Mixed Layer Depth (MLD), Depth of Maximum Stratification (Max N^2 Depth), and DCM With the Depth-Integrated Chlorophyll (intChl) Anomaly, and Also With the Depth-Integrated NPP (intNPP) Anomaly, Only Correlations With $p \leq 0.05$ Are Reported

	Max N^2	MLD	Max N^2 depth	DCM
intChl				
AS	0.13, −0.21	0.54	0.52	−0.25
BoB	0.32	0.52	0.10, −0.25	−0.48
EIO	0.52, −0.28	0.55	−0.50	−0.71
intNPP				
AS	0.07, −0.14	0.16, −0.20	0.25, −0.26	0.23, −0.26
BoB	none	0.46	0.10, −0.33	−0.15
EIO	−0.30	0.24, −0.14	0.10, −0.54	0.23, −0.23

S3 in Supporting Information S1). No spatial bins in the AS had significant negative trends in max N^2. In the EIO, four bins showed positive trends with a maximum value of 4.2×10^{-4} $s^{-2}year^{-1}$ and a minimum value of 2×10^{-4} $s^{-2}year^{-1}$. These bins contained six to 8 years of data. There were two spatial bins in the EIO that showed negative trends (largest -8×10^{-4} $s^{-2}year^{-1}$ and smallest -6.4×10^{-4} $s^{-2}year^{-1}$). The negative trends were mostly observed in the southeastern equatorial region between 5°S and 10°S latitudes. However, these bins contained only 2 to 3 years of data and probably do not resolve trends well, even though they are significant. Within the three regions, the BoB had the highest number of spatial bins with positive trends in max N^2, but the positive trends calculated on the data from the EIO indicated a slightly stronger increasing trend in stratification strength overall. The analysis also showed that the temperature component of stratification was more dominant than the salinity component. In the AS, a comparison between August 2017 and August 2022 showed temperature-to salinity contribution ratios of 14.74 and 13.97, respectively. In the BoB, the comparison between August 2015 and August 2018 resulted in ratios of 4.05 and 3.92. For the EIO, the comparison between August 2014 and August 2021 showed ratios of 9.20 and 8.57, respectively. The month of August was selected as it corresponds to the peak discharge of the Ganges-Brahmaputra river system relative to other months. Not all years in each bin contain data for every month; therefore, only the years that include data for August were used for the comparison in each basin. These results indicated that, although the temperature contribution remained dominant, its influence on stratification has slightly decreased over time, while the salinity contribution had increased marginally.

Generally, the MLD was not subject to significant change across the study region (Figure 7b), with only four spatial bins exhibiting significant positive trends and only one bin with a significant negative trend. In the AS, two spatial bins in the middle of the basin had significant positive trends in MLD (the maximum of 2.0 m yr^{-1} and minimum of 0.8 m yr^{-1}). Those bins had 9 (bin number 14) to 10 years (bin number 5) of data (Figure S3 in Supporting Information S1). In the BoB, one spatial bin on the western side of the basin, which contained 5 years of data, had a significant positive trend with a value of 2.1 m yr^{-1}. In the EIO, only one spatial bin showed a significant negative trend in MLD anomaly (−3.0 m yr^{-1}) and contained 5 years of data, while one spatial bin had a significant positive trend (1.4 m yr^{-1}) and contained 9 years of data.

3.3. Correlations Between Water Column Structure and Depth-Integrated Chlorophyll

We calculated the correlations between parameters describing the vertical structure of the water column (anomalies of maximum N^2, MLD, DCM) and depth-integrated chlorophyll and NPP anomalies, separately. After calculating the correlation coefficient for each spatial bin, only the spatial bins where significant correlations were observed were considered, and the strongest statistically significant correlations observed within each region (AS, BoB, EIO) are reported in Table 3.

The correlation between maximum N^2 anomaly and the depth-integrated chlorophyll anomaly, mostly showed positive correlations in the BoB, and negative correlations in the AS and the EIO (Figure 8a, Table 3). In the AS, three spatial bins showed a weak negative correlation (strongest correlation, $r = -0.21$), and one spatial bin showed a weak positive correlation, $r = 0.13$ (Table 3). All of the bins with statistically significant correlations in the BoB showed weak positive correlations (strongest correlation, $r = 0.32$). The western part of the BoB showed a slightly more positive correlation than the eastern part. In the EIO, four spatial bins had a weak negative correlation (strongest correlation, $r = -0.28$). Two spatial bins in the EIO showed a moderate positive correlation; the strongest r value was 0.52 (Table 3).

Five spatial bins had a significant but moderate positive correlation between the depth of the maximum N^2 anomaly and the depth-integrated chlorophyll anomaly in the AS; the highest correlation was $r = 0.52$ (Figure 8b). In the BoB, only one spatial bin situated in the north-central part had a weak positive correlation, $r = 0.10$, and three spatial bins had a weak negative correlation (Table 3, the strongest r value was −0.25). However, in the EIO nine spatial bins had a significant moderately weak negative correlation and the strongest correlation in those

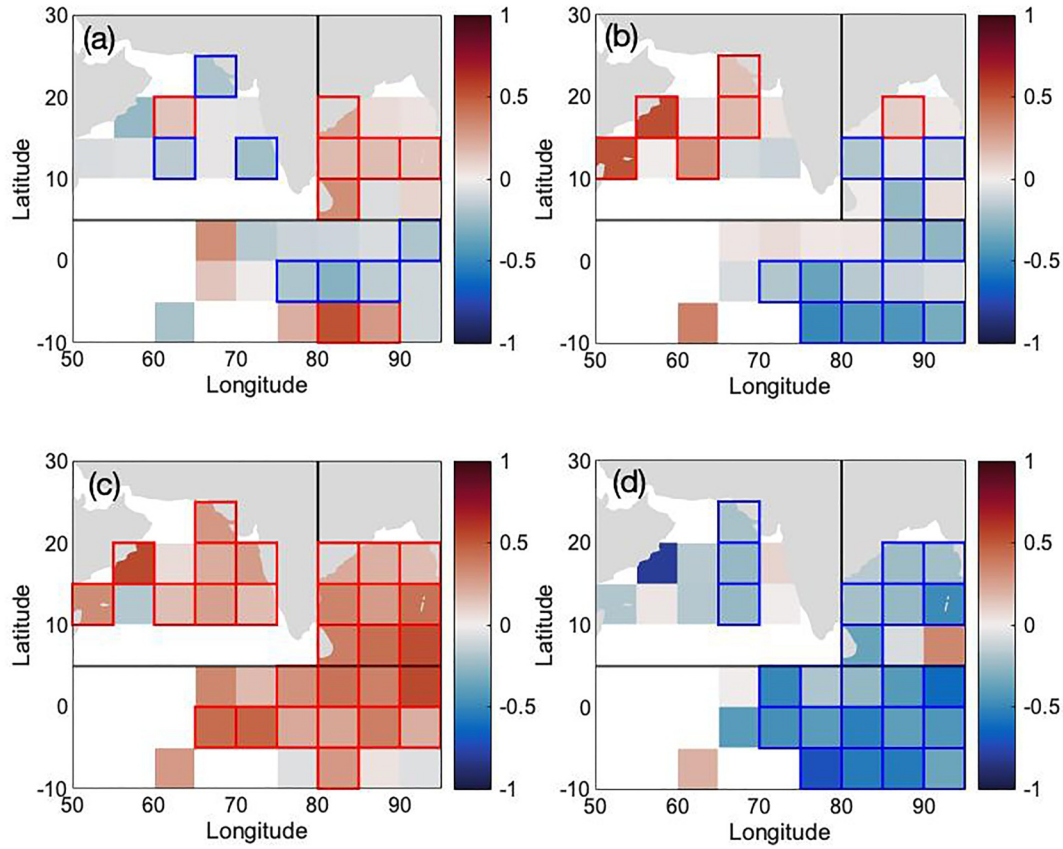

Figure 8. Correlation of anomalies of (a) stratification strength (maximum N^2), (b) depth of maximum stratification, (c) mixed layer depth (MLD) and (d) deep chlorophyll maximum (DCM) with depth-integrated chlorophyll (intChl) anomaly, $p \leq 0.05$ significance. The spatial bins with red borders indicate significant positive correlation and the spatial bins with blue border indicate significant negative correlation. The black lines separate three different regions of Arabian Sea, Bay of Bengal, and Equatorial Indian Ocean.

spatial bins was $r = -0.50$ (Table 3). The results suggest that the AS and the EIO have an opposite relationship between depth-integrated chlorophyll and depth of maximum N^2 anomalies.

We found that over the whole study region, there was a statistically significant weak to moderate positive correlation between the MLD and depth-integrated chlorophyll anomalies (Figure 8c). In the AS, there were eight spatial bins (strongest correlation, $r = 0.54$) which were significant. There were nine significant spatial bins in the BoB (strongest correlation, $r = 0.52$) and 11 significant spatial bins in the EIO (Table 3, strongest correlation $r = 0.55$). The correlation coefficient values suggested that the strength of the correlation between the MLD and depth-integrated chlorophyll anomalies was similar (Table 3) among all parts of the Indian Ocean.

The study region had a mostly weak/moderate negative correlation between the DCM and depth-integrated chlorophyll anomalies (Figure 8d). This correlation was strongest in the EIO where 14 spatial bins had a significant moderate negative correlation, and the strongest correlation within these 14 spatial bins was $r = -0.71$ (Table 3). There were three spatial bins in the eastern AS and six spatial bins in the BoB which had a significant weak negative correlation. The strongest correlations in the AS and the BoB were $r = -0.25$ and $r = -0.48$, respectively (Table 3). The AS had a weaker correlation between the DCM and depth-integrated chlorophyll anomalies than the BoB and the EIO.

The correlation between the maximum N^2 anomaly and depth-integrated NPP anomaly showed no significant correlation in the BoB (Figure 9a). Only two spatial bins had weak negative correlations in the EIO (Table 3, strongest correlation $r = -0.30$). In the AS, one spatial bin showed a positive and one spatial bin showed a negative correlation, which were both very weak. The correlation between the depth of maximum N^2 anomaly and

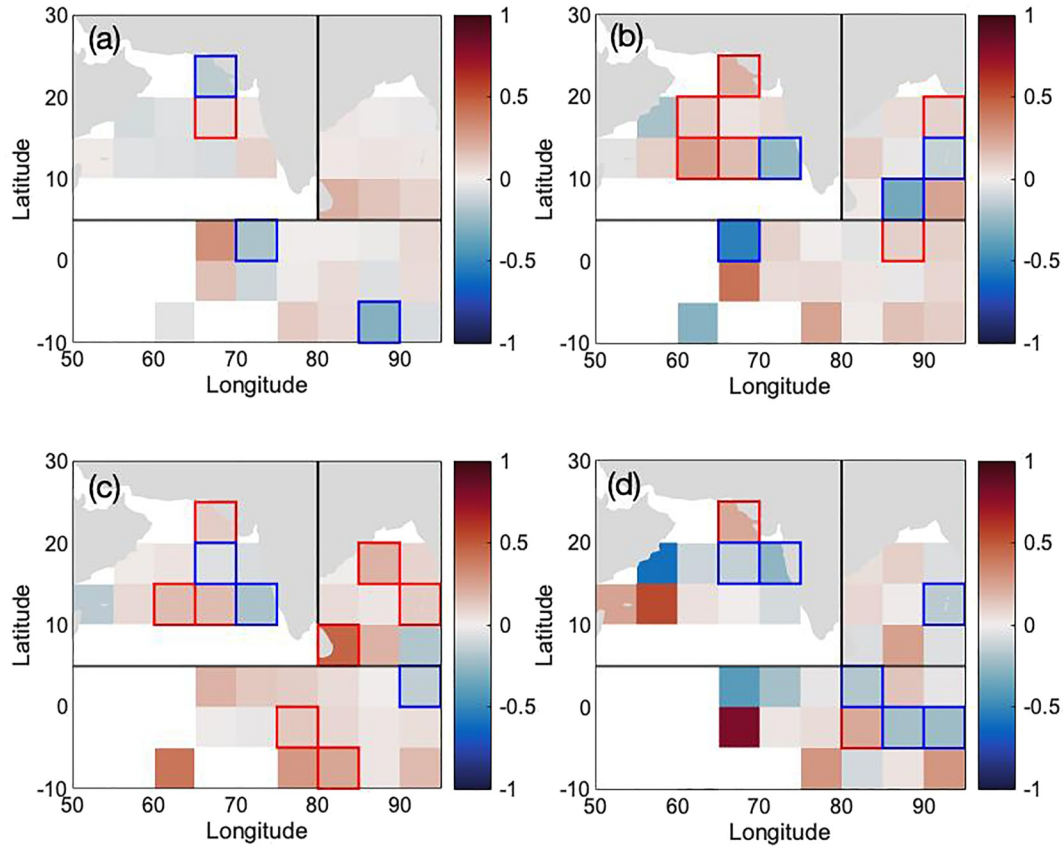

Figure 9. Correlation of anomalies of (a) stratification strength (maximum N^2), (b) depth of maximum stratification, (c) mixed layer depth (MLD) and (d) deep chlorophyll maxima (DCM) with depth-integrated NPP (intNPP) anomaly, $p \leq 0.05$ significance. The spatial bins with red/blue borders indicate significant positive/negative correlations. The black lines separate three different regions of Arabian Sea, Bay of Bengal, and Equatorial Indian Ocean.

the depth-integrated NPP anomaly (Figure 9b) mostly (four spatial bins) showed a weak positive correlation in the AS (strongest correlation, $r = 0.25$) and showed both positive and negative weak correlations in the BoB and in the EIO. The BoB had a moderate positive correlation between MLD and depth-integrated NPP (Figure 9c) in three significant spatial bins (strongest correlations, $r = 0.46$). The EIO mostly showed a positive correlation; however, only two spatial bins had a significant weak positive correlation and only one bin had a significantly weak negative correlation between MLD and depth-integrated NPP. Three spatial bins showed weak positive and two spatial bins showed a weak negative correlation in the AS. Between the DCM anomaly and depth-integrated NPP anomaly (Figure 9d), only one spatial bin in the BoB showed a weak negative correlation (Table 3, $r = -0.15$). Three spatial bins had weak negative (strongest correlation $r = -0.23$), and one bin had weak positive correlation ($r = 0.23$) in the EIO. In the AS, two spatial bins had a weak negative and one bin had a weak positive correlation between the DCM anomaly and depth-integrated NPP anomaly.

3.4. Climate Mode Impacts on Depth-Integrated Chlorophyll

During our study period, 2015 and 2019 were positive IOD years and 2016 and 2022 were negative IOD years. An El Niño occurred in 2016 and La Niña in 2021 and 2022. We found that the correlation between depth-integrated chlorophyll anomaly and the IOD index varied regionally among the AS, BoB, and EIO (Figure 10a). In the AS, two spatial bins exhibited a weak positive correlation (strongest correlation, $r = 0.14$) and three spatial bins in this region had a weak negative correlation (strongest correlation $r = -0.22$). The negative correlations were mostly found in the northeastern part of the AS. In the BoB, two spatial bins had a weak positive correlation (strongest correlation $r = 0.22$) and three spatial bins had a weak negative correlation (strongest correlation $r = -0.30$). The negative correlations were mostly located in the northeastern part of the BoB. In the EIO, four spatial bins had a weak positive correlation (strongest correlation $r = 0.30$), situated at the eastern side of the EIO and one spatial

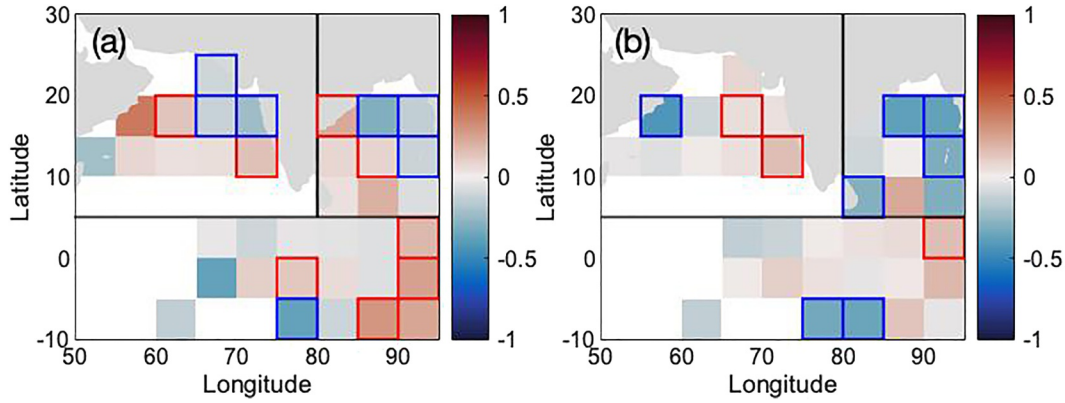

Figure 10. Correlation of (a) IOD and (b) ENSO with depth-integrated chlorophyll (intChl) anomaly, $p \leq 0.05$ significance. The spatial bins with red/blue borders indicate significant positive/negative correlations. The black lines separate three different regions of Arabian Sea, Bay of Bengal, and Equatorial Indian Ocean.

bin had a moderate negative correlation, $r = -0.37$. In all three basins, correlations were mostly weak between depth-integrated chlorophyll anomaly and the IOD index.

In the AS, the correlation between the depth-integrated chlorophyll anomaly and ENSO (Figure 10b) was statistically significant in three spatial bins. Within these three spatial bins, two had a weak positive correlation (strongest correlation $r = 0.15$) and one spatial bin had a moderate negative correlation ($r = -0.42$). Positive correlations were mostly observed in the eastern part of the AS, whereas negative correlations were found in the western part of the AS. In the BoB, four spatial bins had a weak negative correlation (strongest correlation $r = -0.38$). In the EIO, two spatial bins had weak negative correlation (strongest correlation $r = -0.35$) and only one spatial bin had a weak positive correlation ($r = 0.15$) which was situated in the eastern part of the EIO. Within all three basins, the depth-integrated chlorophyll anomaly was more negatively correlated with ENSO in most parts of the BoB than in the AS or the EIO.

The correlation between the depth-integrated NPP anomaly and the IOD index varied regionally between the AS, BoB, and EIO (Figure 11a). In the AS, three spatial bins exhibited a weak negative correlation (strongest correlation $r = -0.2$) and one spatial bin had a weak positive correlation ($r = 0.13$). The negative correlations were mostly observed in the northeastern part of the AS. In the BoB, three spatial bins had a weak negative correlation (strongest correlation $r = -0.23$) and one spatial bin had a weak positive correlation ($r = 0.33$). The negative correlations were mostly located in the northeastern part of the BoB. In the EIO, three spatial bins had weak positive correlation (strongest correlation $r = 0.33$), generally located at the eastern part of the EIO.

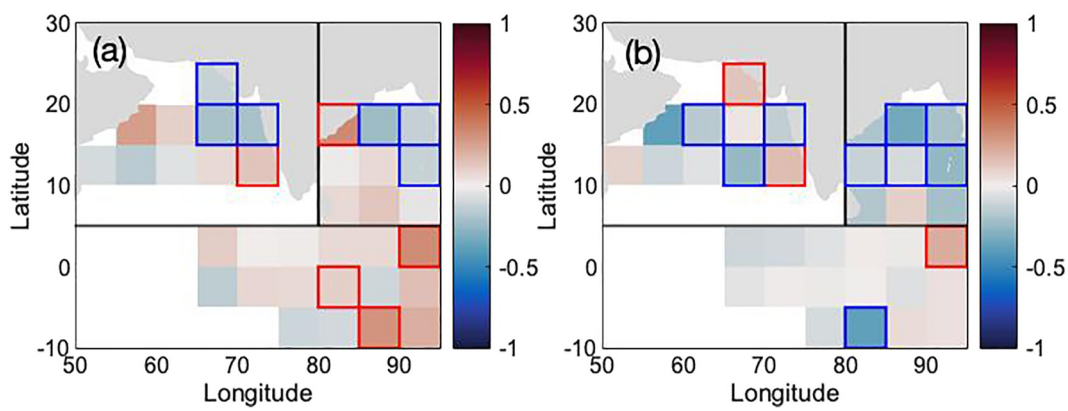

Figure 11. Correlation of (a) IOD and (b) ENSO with depth-integrated NPP (intNPP) anomaly, $p \leq 0.05$ significance. The spatial bins with red/blue borders indicate significant positive/negative correlations. The black lines separate three different regions of Arabian Sea, Bay of Bengal, and Equatorial Indian Ocean.

In the AS, the correlation between depth-integrated NPP anomaly and ENSO (Figure 11b) was statistically significant in five spatial bins. Within these, two had weak positive correlations (strongest correlation $r = 0.16$) and three spatial bins had weak negative correlations (strongest correlation $r = -0.25$). In the BoB, five spatial bins had a weak negative correlation (strongest correlation $r = -0.33$). In the EIO, one spatial bin had a weak negative correlation situated at the southern part ($r = -0.38$) and one spatial bin had a weak positive correlation ($r = 0.21$) which was situated in the eastern part of the EIO. Within all three basins, the depth-integrated NPP anomaly was more negatively correlated with ENSO in most parts of the BoB than in the AS or the EIO.

4. Discussion

4.1. Regional and Seasonal Variability in Chlorophyll, NPP, MLD, DCM, and Stratification

In the AS, both surface and depth-integrated chlorophyll concentrations are higher during monsoon seasons (summer monsoon months of June through September, and the winter monsoon months of November through February) compared to the inter-monsoon. Our study finds that in the AS the surface chlorophyll ranges from 0.2 mg m^{-3} to 0.8 mg m^{-3} and the maximum surface and depth-integrated chlorophyll occur in December (Figure 2). A previous study, based on data from only two BGC-Argo floats in the AS also found higher chlorophyll concentration during summer and winter monsoons with particularly high chlorophyll during January-February, and peak concentrations of surface chlorophyll around 0.4–0.6 mg m^{-3} (Jayaram et al., 2021). Peak surface and depth-integrated chlorophyll concentrations during the summer monsoon are mostly driven by upwelling along the Somalia coast along with positive wind stress curl which makes the mixed layer deeper (Figure 4a) and drives upward transport of nutrients that enhances productivity (Lakshmi et al., 2020). Advection of these upwelled nutrients together with the positive wind stress curl and associated mixing and Ekman pumping enhance productivity in the central AS (S. P. Kumar et al., 2009; Thushara & Vinayachandran, 2020). Higher surface and depth-integrated chlorophyll in the AS during winter is due to the enhanced convective mixing by dry northeasterly winds that enhance evaporative cooling and deepen the mixed layer (Figure 4a), which results in the entrainment of nutrients toward the surface, thereby enhancing productivity (Prasanna Kumar et al., 2009; Thushara & Vinayachandran, 2020).

In the BoB, the range of monthly mean surface and depth-integrated chlorophyll is lower compared to the AS and the EIO. Surface chlorophyll ranges from 0.1 mg m^{-3} to 0.3 mg m^{-3} in the BoB which is consistent with reported values of 0–0.3 mg m^{-3} (Jayaram et al., 2021), where a smaller set of BGC-Argo profile data from this region were used. Our results show a semi-annual seasonality in both surface chlorophyll and depth-integrated chlorophyll which peaks during the summer and winter monsoons (Figure 2). This study is based on a larger set of observations in time and space than previously available, allowing for better resolution and identification of seasonal patterns. During summer, a large freshwater flux and enhanced precipitation result in lower surface salinity and strong density stratification, which in turn leads to weak vertical mixing (Jayaram et al., 2021). However, the higher surface and depth-integrated chlorophyll observed during summer in the BoB is likely due to upwelling by the local alongshore wind stress, wind driven mixing and eddy pumping (Thushara et al., 2019) which erode the stratification. Higher surface and depth-integrated chlorophyll during winter is driven by the northeasterly wind-driven Ekman pumping that fuels upwelling and entrains nutrients from deep waters into the surface (Xu et al., 2021). Mesoscale eddies could also supply nutrients and enhance chlorophyll biomass (S. P. Kumar et al., 2009). During summer and winter, the MLD in the BoB is deeper (Figure 4b) which explains the higher chlorophyll and NPP.

In the EIO, we observe no strong seasonality in surface and depth-integrated chlorophyll (Figure 2), and chlorophyll concentrations in the EIO are generally higher than the BoB, but lower than the AS (Dalabehara & Sarma, 2021). Our study shows lower surface chlorophyll during pre-monsoon (lowest in March; 0.30 $\pm$ 0.21 mg m^{-3}) and slightly higher surface chlorophyll in winter (0.33 $\pm$ 0.24 mg m^{-3} in November) by averaging over 10 years. This result differs somewhat from a previous study based on MODIS data from 2002 to 2011, which identified a weak annual cycle in surface chlorophyll, with high surface chlorophyll concentrations in winter (0.22 mg m^{-3}, December 2005) and low in summer (0.07 mg m^{-3}, June 2012) (G. S. Kumar et al., 2016). Their data coverage, sources, and time frame are different from ours.

The comparison of the three basins shows that during December, surface and depth-integrated chlorophyll concentrations are highest in the AS and the BoB. However, in the EIO, this peak occurs a month earlier, in

November (Table 1). Moreover, the summer peak in the BoB occurs in July, while in the AS, this peak is observed a month later, in August. Similarly, the lowest values are seen in April and September in the BoB, whereas, in the AS, the lowest values occur a month later, in May and October. The earlier occurrence of high chlorophyll values in the BoB could be attributed to riverine input that carry nutrients (Amol et al., 2020; Pedde et al., 2017) and can lead to an earlier phytoplankton bloom. Additionally, strong stratification in the BoB, which can trap nutrients in the surface layer, may also play a role.

NPP follows a similar pattern to chlorophyll in the AS (Figure 3), with higher productivity during the monsoon seasons (Vinaya Kumari et al., 2021). NPP is lower in the BoB than the AS and the seasonality follows the pattern of chlorophyll. Although surface NPP in the EIO shows no clear seasonality, depth-integrated NPP is slightly higher during summer-fall and lower during winter-spring (Figure 3). This likely reflects the inclusion of DCM-associated productivity in depth-integrated NPP. Previous work based on ^{13}C incubation for assessing productivity from 25 locations during April–May 2014 found that depth-integrated production in the photic zone was higher in the AS (1483 ± 202 mg C m^{-2} d^{-1}) followed by the EIO (1182 ± 360 mg C m^{-2} d^{-1}) and BoB (878 ± 390 mg C m^{-2} d^{-1}) (Dalabehara & Sarma, 2021). Our study reports higher mean April–May depth-integrated NPP in the EIO (1145 ± 552 mg C m^{-2} d^{-1}), than in the AS (944 ± 606 mg C m^{-2} d^{-1}) and lower in the BoB (650 ± 469 mg C m^{-2} d^{-1}).

Our results show the MLD and the DCM in the AS have a semi-annual pattern (Figure 4a), with the MLD deepening during the monsoon seasons due to strong winds and convective mixing (Bhaskar et al., 2007). As the mixed layer deepens, the DCM shoals and approaches the MLD, likely due to convective mixing that can inject nutrients into the surface layer. The depth of maximum stratification mostly follows the same pattern as the MLD in the AS, with stronger stratification observed during the summer monsoon (Figure 5).

In the BoB, the MLD has a semi-annual pattern, whereas the DCM has an annual pattern (Figure 4b). The DCM is deeper during the pre-monsoon season (March-May) while, by contrast, the MLD is shallower. During the summer monsoon and winter monsoon, the MLD deepens while the DCM shoals (Jayaram et al., 2021). Even though the DCM shoals, it never reaches the surface due to stratified water. In situ measurements from the southern BoB during the summer monsoon in 2016 found that the depth of the DCM ranged from 20 to 50 m (Thushara et al., 2019), which is shallower than the estimated mean summer monsoon DCM depth (55–65 m) obtained in our study. During September-October, the stratification becomes stronger and the depth of maximum stratification shoals to around 50 m (Figure 5) and the DCM also shallows to around 54 m (Figure 4). The DCM coincided with the depth of maximum stratification (Somavilla et al., 2019) in the BoB and is located below the mixed layer (Jayaram et al., 2021) throughout the year.

In the EIO, the DCM and MLD both follow an annual cycle that shoals during the winter monsoon and deepens during the summer monsoon, with the DCM mostly following the same pattern as the MLD except in August when the MLD is deepest and the DCM shoals somewhat (Figure 4c). Our study finds that the mean monthly MLD ranges from 22 to 42 m in the EIO, while Keerthi et al. (2016) reported MLD variations between 20 and 30 m, which are linked to the annual wind cycle which influences stirring effects and buoyancy fluxes. Throughout the year stratification is strong in the EIO (Figure 5) but the depth of maximum stratification shoals during the pre-monsoon (March–May).

4.2. To What Extent Does Stratification Control Depth-Integrated Chlorophyll?

There is a widely held view that the strength of stratification in the water column plays a major role in controlling primary production and the variability of chlorophyll in the ocean; however, our results suggest that the relationship between stratification and productivity in the Indian Ocean is not straightforward. We find that the correlations between temporal trends in stratification, depth-integrated chlorophyll and NPP vary considerably across the study region. Using all available BGC-Argo float data from a 10-year period, we did not find a strong correlation between stratification and depth-integrated chlorophyll in the northern and Equatorial Indian Ocean. In previous work examining correlations between in situ measurements of stratification and satellite chlorophyll over the global ocean from 1997 to 2013, no evidence of strong correlation between stratification and chlorophyll in the subtropical ocean was found (Dave & Lozier, 2013). Depth-integrated chlorophyll anomaly mostly has a weak negative correlation with stratification in the AS and the northern part of the EIO, and a weak positive correlation in the BoB, central AS, and southern part of the EIO (Figure 8). A positive correlation indicates that

even if there is an increase in stratification that might inhibit increases in surface chlorophyll, it can still result in increases in subsurface chlorophyll which satellite measurements cannot detect (Xu et al., 2021). We found only three spatial bins that show a significant weak negative correlation between depth-integrated NPP and stratification, mostly in the EIO (Figure 9), indicating decreases in NPP concurrent with increases in stratification. Sridevi et al. (2023) used satellite data from 2001 to 2020 and observed a decline in NPP south of 12°N. They found an inverse correlation between NPP and SST, suggesting that weak nutrient supply due to stratification controls NPP. However, in most parts of our study area, depth-integrated NPP is not significantly correlated with stratification (Figure 9), suggesting that the relationship between stratification and productivity is localized and variable, rather than having a consistent effect across the entire northern and Equatorial Indian Ocean.

Depth-integrated chlorophyll anomaly has a moderate positive correlation with MLD anomaly and a moderate negative correlation with DCM anomaly in the AS, BoB, and EIO. This indicates that the depth-integrated chlorophyll increases when the MLD becomes deeper or/and when DCM becomes shallower (Figure 8). The decline in depth-integrated chlorophyll is linked to the shoaling of the mixed layer, as a shallower mixed layer can reduce the supply of nutrients from the deep ocean to the surface (Gregg & Rousseaux, 2019). A shallow DCM typically indicates greater light attenuation and enhanced nutrient availability at shallower depths, which leads to higher chlorophyll concentrations (Mignot et al., 2014). Depth-integrated NPP anomaly mostly has a significant weak positive correlation with MLD and a significant weak negative correlation with DCM, but this relationship varies throughout the basin (Figure 9).

We find that temporal trends in depth-integrated chlorophyll and NPP differ between the eastern and western AS (Figure 6). Chlorophyll in the AS is largely invisible to satellites during the most productive period of the year (e.g., the summer monsoon) due to cloud cover (Modi & Koll, 2023). Prakash and Ramesh (2007) noted that the surface chlorophyll trend in the western AS, reported by Goes et al. (2005), differs from that in the eastern AS. The eastern AS has a decreasing trend in depth-integrated chlorophyll and depth-integrated NPP of up to 6% (based on the maximum significant negative trend) per year. Not all spatial bins contain 10 years of available profile data (Figure S3; Table S1 in Supporting Information S1). There are three bins which have 10 years of data, and three other bins have seven and 9 years of data. Sridevi et al. (2023) reported a 22% annual decline in NPP in the northeastern AS based on satellite chlorophyll data from 2001 to 2020. Gregg and Rousseaux (2019) assimilated ocean color satellite data into an ocean biological model, and their study suggested a decline in NPP in the eastern AS from 1998 to 2015. Vinaya Kumari et al. (2021) also found a decline in NPP in the eastern AS in the 2007–2016 period, based on an analysis of satellite data, which they attributed to a concurrent increase in SST. In the western AS, by contrast, an increasing trend was observed in depth-integrated chlorophyll of up to 7% (based on the maximum significant positive trend) per year and a rise in depth-integrated NPP of up to 11% (based on the maximum significant positive trend) per year. This enhancement in production possibly due to the external nutrient inputs, which can result from increased atmospheric deposition such as dust (Kuttippurath et al., 2023) and aerosols in the AS (Sridevi et al., 2023) or from enhanced upwelling (Löscher, 2021).

In the BoB, we observe an increasing trend in both depth-integrated chlorophyll and depth-integrated NPP (Figure 6). Although only one spatial bin has 10 years of data and all other significant bins have 5 to 7 years of data (Figure S3; Table S1 in Supporting Information S1), the depth-integrated chlorophyll shows mostly positive trends, with the rate of increase being slightly higher in the northwestern BoB (15% increase per year; based on the maximum significant positive trend). Similarly, a global analysis of satellite chlorophyll trends, based on the Copernicus Marine Environment Monitoring Service product from 1997 to 2021, also identified an increasing trend in surface chlorophyll in the western BoB (Sathyendranath et al., 2019), which supports the findings of our study. Multi-satellite merged chlorophyll data from 1998 to 2019 also revealed a positive trend in NPP in the western BoB (Kuttippurath et al., 2023). There is only one spatial bin in the northern BoB, which has a significant 5% decrease of depth-integrated chlorophyll per year (Figure 6). Our results show that the depth-integrated NPP is significantly increasing at a rate of up to 28% (based on the maximum significant positive trend) per year in the north-western part of the BoB, supported by previous modeling work which found an increasing surface NPP trend in the central BoB using Coupled Model Intercomparison Project (CMIP6) model output for 2003 to 2014 (Sunanda et al., 2023). Enhanced atmospheric aerosols and river discharge, which have been shown to boost nutrient supply, may play a significant role in the observed increase in NPP in the BoB (Sridevi et al., 2023).

Considering only significant spatial bins, which mostly contains 6 to 9 years of data (Figure S3; Table S1 in Supporting Information S1), our study shows that the EIO has seen an up to 6% (based on the maximum

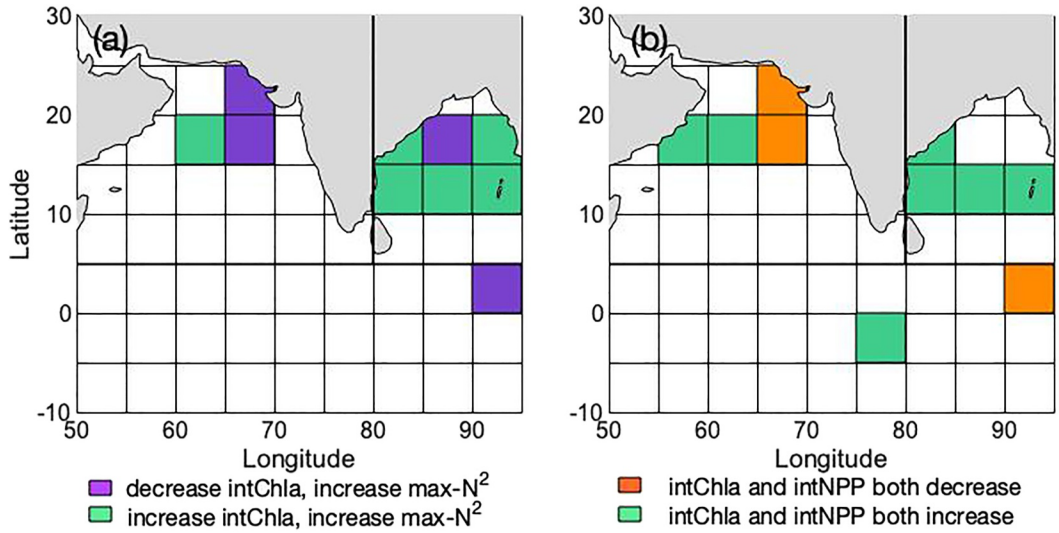

Figure 12. Summary of trends showing only the significant spatial bins (a) decrease of depth-integrated chlorophyll (intChl) anomaly and increase of max-N^2 anomaly (purple) and both depth-integrated chlorophyll (intChl) anomaly and max-N^2 anomaly are increasing (green); (b) depth-integrated chlorophyll (intChl) anomaly and depth-integrated NPP (intNPP) anomaly both are increasing (green) and both are decreasing (orange).

significant positive trend) increase and up to 25% (based on the maximum significant negative trend) decrease per year in depth-integrated chlorophyll (Figure 6). This decrease is most prominent in the eastern part of the EIO, and overall, negative trends dominate in this basin. Using monthly satellite-derived chlorophyll data, G. S. Kumar et al. (2016) and Gregg and Rousseaux (2019) found a decreasing trend in the EIO for the periods 2002–2012 and 1998–2015, respectively. Depth-integrated NPP in the EIO shows a larger decrease (45%; based on the maximum significant negative trend) than increase (6%; based on the maximum significant positive trend) per year. This decreasing trend is likely driven by enhanced ocean stratification due to the rapid warming in the Indian Ocean (Roxy et al., 2014), which could reduce the upwelling of the nutrients and suppress NPP (Gregg & Rousseaux, 2019).

Our study, based on observational data, has shown that stratification is mostly increasing in the northern Indian Ocean, challenging previous work which found that stratification decreased in the BoB and the EIO and increased in the northwest AS (Dave & Lozier, 2013). The stratification is increasing (Figure 7) at a rate of up to 5% (based on the maximum significant positive trend) per year in the AS. Not all spatial bins have 10 years of data in AS, BoB, and EIO (Figure S3, Table S1 in Supporting Information S1). However, a total of 26 bins have at least five years of data, which can be used to identify short-term trends. There is also the possibility that the observed trends are driven by inter-annual/decadal climate variability rather than longer-term change (Behrenfeld et al., 2006). We acknowledge the limitation imposed by the shorter time series in this study and believe that continued data collection using BGC-Argo will increase confidence in trend analysis of this region. In the BoB, stratification has mostly positive trends (18% increase per year; based on the maximum significant positive trend); only one spatial bin at the southern BoB (Figure 7a) has an 15% decrease in stratification per year. Yamaguchi and Suga (2019) investigated the upper ocean stratification (density difference between surface and 200-m depth trends) from observational profiles for the years 1960–2017 and they found an increasing trend of stratification in the BoB and that the stratification is increasing more in the BoB and eastern EIO compared to the AS. Our study shows that stratification has both positive and negative trends (Figure 7) in the EIO. At the northeastern EIO stratification is increasing; however, at the southeastern side stratification is decreasing. The decrease of stratification could be attributed to a faster rate of subsurface warming compared to the surface warming, as previously discussed (Dave & Lozier, 2013; Roxy et al., 2016). Temperature remains the dominant contributor to stratification; however, its influence is decreasing, while the contribution of salinity has increased to a limited extent. In this study region, there are few significant trends in MLD. Only four spatial bins show a deepening of the mixed layer (Figure 7). In the EIO, just one spatial bin exhibits a 10% per year decrease in MLD. These MLD changes are primarily linked to surface buoyancy forcing and wind stirring (Gao et al., 2023).

Our analysis of the temporal trends of depth-integrated chlorophyll anomaly and max-N^2 anomaly identifies two scenarios: a decreasing trend in depth-integrated chlorophyll co-occurring with an increasing trend in stratification, and an increasing trend for both depth-integrated chlorophyll and stratification (Figure 12a). The first scenario is observed in the AS, BoB, and in the EIO, whereas the second scenario is more prevalent in the BoB. When water column stratification increases, it can act to reduce upward nutrient fluxes from depth thereby reducing productivity and observed chlorophyll concentrations (Cermeño et al., 2008; Li et al., 2020), unless nutrients are not limiting growth or there is a sufficient local supply of nutrients within the surface mixed layer. Martinez et al. (2009) used monthly satellite observation of surface chlorophyll and sea surface temperature (as an indicator of stratification) and reported that most of the Indian Ocean (around 61%) had a parallel increase in chlorophyll and sea surface temperature (SST) during 1979–1983 to 1998–2002. Though their period does not line up with our study, our results show that a parallel increase in both stratification and depth-integrated chlorophyll is found in the BoB (Figure 12a). Though Dave and Lozier (2013) found a significant decrease of both stratification and surface chlorophyll at the eastern EIO; our study did not find any significant relationship there.

We identify two scenarios based on the temporal trends of depth-integrated chlorophyll and depth-integrated NPP: first where both are decreasing, and second where both are increasing. In the AS, both depth-integrated chlorophyll and depth-integrated NPP are significantly increasing in two spatial bins (Figure 12b) on the western side and decreasing in two spatial bins on the eastern side. We hypothesize that the decreasing scenario in the AS is driven by the concurrent increase in stratification (Figure 12a). Conversely, we attribute the increasing trend in depth-integrated chlorophyll and NPP in the western AS to rising dust concentrations, driven by winds transporting dust from the Arabian and Mediterranean regions. This increase in atmospheric dust during 1998–2019 overlaps with this study period by 7 years (Kuttippurath et al., 2023), lending further support to this hypothesis. In the BoB, both depth-integrated chlorophyll and NPP anomaly increase significantly (four spatial bins; Figure 12b). There is a decline in the Himalaya glacier with an enhanced decreasing trend since the 1990s (Dimri et al., 2021) which results in an increase in river discharge to the BoB, which is a source of nutrients (Krishna et al., 2016). Apart from nutrients supplied by the Ganges-Brahmaputra river system and wind-driven upwelling and vertical mixing, atmospheric dust deposition (Siswanto et al., 2023) is also an important source of inorganic nutrients, especially in the central/eastern BoB and those dust depositions intrude into the BoB from the southwest. Dust concentrations show the highest values near the western BoB (Kuttippurath et al., 2023). Moreover, the deposition of nutrients from aerosols can compensate for the declining trends of NPP due to warming (Sridevi et al., 2023). Aerosols are mainly transported from the Indo-Gangetic Plain and the distribution decreases towards the east and southern BoB (Kuttippurath et al., 2023). Another possible reason could be cyclones and cyclonic eddies, that are generated in the BoB and can intensify Ekman divergence, thus supplying more nutrients which can enhance chlorophyll (Jayaram et al., 2019). In the EIO, one spatial bin in the northeast shows a decrease, while one spatial bin in the central EIO shows an increase in both depth-integrated chlorophyll and depth-integrated NPP (Figure 12b). Over South and Southeast Asia, atmospheric pollutants are increasing rapidly since the middle of the 1990s (Kurokawa & Ohara, 2020). It was observed that between 2001 and 2020 due to an increase in anthropogenic pollutants over South and Southeast Asia, there is an increase in aerosol mass load, nitrate and ammonium concentrations and 27%–30% of the primary production in the northern Indian Ocean is contributed by the atmospheric deposition of nutrients (Sarma et al., 2022).

Atmospheric deposition is generally considered a minor nutrient source in the northern Indian Ocean (Singh et al., 2012) compared to oceanic processes such as mixing and upwelling. However, recent evidence suggests that nitrogen deposition can partially compensate for climate-driven reductions in primary productivity in certain regions, particularly in the central AS and the western BoB (Malsang et al., 2024), and thus modulate regional productivity trends despite increasing stratification. Increased atmospheric deposition might account for the positive trend in chlorophyll and NPP that we observed in the BoB and in the central and western AS. The observed chlorophyll trends in the northern Indian Ocean are likely driven by a combination of large-scale climate forcing and regional oceanographic processes that regulate nutrient supply to the euphotic zone. In addition to large-scale stratification and monsoon-driven mixing, changes in regional coastal circulation may also play an important role. Recent studies have reported an increased influx of low-salinity water into the eastern AS during 1990–2010, attributed to the strengthening of the Northeast Monsoon Current and the West India Coastal Current (Varna et al., 2021). Our study shows an increase in stratification in the eastern AS, which may be connected to this increasing influx of low-salinity water. We also observed a decrease in chlorophyll and NPP in this region,

likely due to reduced vertical mixing. Changes in monsoonal patterns associated with land-sea temperature contrasts are therefore expected to influence this region (Prakash & Ramesh, 2007). Variability in coastal circulation and alongshore wind forcing can substantially alter upwelling intensity and cross-shelf transport, thereby modulating nutrient supply and biological productivity. Changes in zonal winds and thermocline depth linked to large-scale climate modes such as the IOD and ENSO may further contribute to regional variability. While the present analysis does not quantify individual mechanisms, the observed chlorophyll trends with these known physical processes suggests that changes in circulation and mixing/stratification likely contribute to the patterns reported here.

4.3. Chlorophyll Response to Climate Variability

Both ENSO and IOD have been shown to significantly influence near-surface physical processes in the northern Indian Ocean, such as upwelling, downwelling, atmospheric circulation and mixing, and therefore it is likely that they will also influence regional patterns in chlorophyll and productivity (Pandey et al., 2019). Although previous work has identified close coupling between inter-annual variability in chlorophyll and IOD and ENSO modes in the northern Indian Ocean (Yin et al., 2022), regional differences in the strength of the effect of these climate modes and their impact on depth-integrated chlorophyll is still not well understood, largely due to a lack of depth-resolved chlorophyll data. In this study, significant regional differences were found in the strength and the sign of the correlation between depth-integrated chlorophyll and NPP and these climate modes (Figures 10 and 11).

In the BoB, both depth-integrated chlorophyll and NPP have a larger weak negative correlation with ENSO than IOD (Figures 10 and 11). The depth-integrated chlorophyll has a weak negative correlation with ENSO in the upwelling region near Sri Lanka ($r = -0.30$). Our study agrees with Siswanto et al. (2023) that the surface chlorophyll in the southwest BoB is negatively correlated ($r = -0.27$) with the Niño3.4 ENSO index. El Niño events can bring in warmer surface water and shorter summer monsoons which in turn can reduce upwelling and result in reduced productivity (Currie et al., 2013; Kao & Yu, 2009; Syroka & Toumi, 2004). Therefore, depth-integrated chlorophyll and NPP is lower (higher) during El Niño (La Niña). Our study also shows that the northern and eastern parts of the BoB have a weak negative correlation with IOD, which indicates depth-integrated chlorophyll and NPP are low (high) during positive (negative) IOD. This is because, during the negative IOD, an enhanced wind curl and anomalously strong cyclonic circulation co-exists in the BoB, which strengthens Ekman pumping, thus resulting in enhanced chlorophyll (Xu et al., 2021). Negative IODs significantly enhance precipitation and river discharge (Pervez & Henebry, 2015) which can bring nutrients. Moreover, more cyclones and cyclonic eddies are generated in the BoB during negative IOD (Mahala et al., 2015), which can intensify vertical mixing and nutrient supply into the euphotic zone and result in increased chlorophyll.

We found that the eastern and western AS respond differently to ENSO and IOD. The eastern AS has a weak positive correlation and western AS shows a moderate negative correlation between depth-integrated chlorophyll anomaly and ENSO (Figure 10b). During El Niño, the western AS experiences warmer SST and a shortened summer monsoon, resulting in a reduced duration of active upwelling and lower productivity (Currie et al., 2013). Using satellite data (OC-CCI) for June–September 1998–2016, Shafeeque et al. (2021) found no significant correlation between chlorophyll and ENSO in the south-eastern AS and indicated that chlorophyll is negatively correlated with IOD. However, our study found a weak positive correlation at the western, southeastern AS and a weak negative correlation at the northeastern AS between the depth-integrated chlorophyll and NPP anomalies and IOD, which agrees with the findings of Sankar et al. (2019). Their study used remotely sensed surface chlorophyll concentration over 1998 to 2014 and found that surface chlorophyll concentration and IOD are significantly negatively correlated in the eastern AS and mentioned that local surface winds in the eastern AS are less favorable for upwelling during positive IOD. Peter et al. (2022) emphasized that the variability of the AS surface circulation and eddy activities during the IOD events can impact the variability of chlorophyll distribution. During a negative IOD, the eastern AS experiences increased Ekman suction, enhanced coastal upwelling, and a shoaling of the thermocline, all of which promote higher chlorophyll concentration (Thushara & Vinayachandran, 2020).

Depth-integrated chlorophyll and NPP in EIO are more significantly correlated with the IOD than ENSO. Our study found a weak positive correlation between depth-integrated chlorophyll and NPP anomalies and IOD in the eastern EIO which is supported by previous findings of Xu et al. (2021). They used chlorophyll data derived from the Moderate Resolution Imaging Spectroradiometer-Aqua, covering the period from January 2003 to December

2018. During a positive IOD, increased wind divergence along the eastern EIO enhances upwelling, boosting chlorophyll concentrations in the region. In contrast, during a negative IOD, the reversal of this forcing anomalies reduces upwelling, leading to lower chlorophyll levels (Xu et al., 2021). The depth-integrated chlorophyll and NPP anomalies in the eastern EIO show a weak positive correlation with ENSO, as also noted by Currie et al. (2013), who used merged satellite chlorophyll data from the European Space Agency's GlobColour project (1998–2009) along with an ocean general circulation model (OGCM). This positive correlation is primarily driven by upwelling of cold, nutrient-rich waters.

Previous work has shown that in the northern Indian Ocean, the influence of El Niño on chlorophyll anomalies is weaker than the influence of IOD based on surface chlorophyll reanalysis data from 1993 to 2007 (Pandey et al., 2019). However, our study based on depth-integrated chlorophyll from BGC-Argo suggests a stronger ENSO impact on chlorophyll variability in this region, comparable to that of the IOD based on the strength of correlations between chlorophyll and these climate modes. Our study also finds that neither depth-integrated chlorophyll nor NPP in the southern AS, southern BoB, and central Equatorial Indian Ocean are significantly correlated with IOD or ENSO (Figure 11).

There is relatively short temporal extent to our data set, which comprises 10 years of data collected across the Indian Ocean. Four spatial bins have 10 years of data, and a total of 26 bins have five or more years of data. Despite the patchy coverage (Figure S3 in Supporting Information S1), there are sufficient data to identify short-term trends in physical and biological water column properties. Longer time series, ideally longer than 40 years, would be needed in order to detect the impact of climate modes on the interannual variability of depth-integrated chlorophyll with confidence (Henson et al., 2010). However, in the absence of such data sets in the Indian Ocean, we believe that the results of this work leveraging a decade of depth-resolved biogeochemical data already serves to highlight the value of the data being collected autonomously by BGC-Argo floats and their continuing role in helping to identify trends in the temporal dynamics of surface ocean productivity.

5. Conclusions

In this paper, we provide a new view of inter-annual trends in depth-integrated chlorophyll abundance and variability in the northern and Equatorial Indian Ocean based on a 10-year time series of depth-resolved data from BGC-Argo floats. Earlier studies focused on surface chlorophyll using remote sensing, modeling, or sparse in situ data sets to understand the seasonal variability and trends in this region. However, with this study we have leveraged a large set of depth-resolved data, which unlike satellite products is not impacted by cloud cover, and gives a fuller view of the distribution of productivity and chlorophyll throughout the whole of the euphotic zone and not just the first optical depth. This work has uncovered spatio-temporal similarities and differences among the AS, BoB, and EIO in terms of surface and depth-integrated chlorophyll and NPP, MLD, DCM, and stratification. We have shown that depth-integrated chlorophyll and NPP both have positive trends in most of the BoB, the western AS, and some parts of the EIO, whereas in the eastern AS, the northern BoB, and other parts of the EIO both have a decreasing trend.

Stratification in the northern Indian Ocean is mostly increasing, and the rate of increase is higher in the western BoB and the eastern EIO. Although temperature remains the dominant factor influencing stratification, its contribution has slightly decreased over time, while the influence of salinity has marginally increased. Stratification is not strongly correlated with depth-integrated chlorophyll and has mostly a weak positive correlation in the BoB, weak negative correlation in the AS, and both weak positive and negative correlation in the EIO. However, in most parts of the study area, depth-integrated NPP is not significantly correlated with stratification, suggesting that the strength of stratification primarily exerts a localized effect on productivity, rather than influencing the entire northern and Equatorial Indian Ocean in a homogeneous way. In the study region, ENSO is equally important along with the IOD; most of the northern Indian Ocean has a weak negative correlation between depth-integrated chlorophyll/NPP and IOD/ENSO. A longer time series and more focused regional analysis are needed to understand how the rapid warming of the Indian Ocean might drive changes in temperature and stratification, and how those will impact surface ocean productivity into the future. Confidence in this trend could be increased through the use of longer data sets and multiple observational sources. However, our results provide preliminary evidence to suggest that increased stratification will not necessarily result in decreased productivity and that in some parts of the Indian Ocean, productivity and chlorophyll concentrations can increase even in the face of increased stratification.

Conflict of Interest

The authors declare no conflicts of interest relevant to this study.

Availability Statement

Publicly available BGC-Argo data were analyzed in this study (https://argo.ucsd.edu/data/). These data were collected and made freely available by the international Argo project and the national programs that contribute to it (Argo, 2026). DMI (IOD Index) data was obtained from https://psl.noaa.gov/data/timeseries/month/DMI/ (N. Saji & Yamagata, 2003). Multivariate ENSO Index Version 2 (MEI.v2) was downloaded from https://psl.noaa.gov/enso/mei/ (Wolter & Timlin, 2011; Zhang et al., 2019). Gibbs-SeaWater (GSW) Oceanographic Toolbox was used in this study and the codes were downloaded from https://www.teos-10.org/ (Li et al., 2020). Surface PAR used from Moderate Resolution Imaging Spectroradiometer (MODIS) products and the monthly data for each year were collected from https://oceancolor.gsfc.nasa.gov (Yang et al., 2022). MATLAB codes of Mann-Kendall Tau-b with Sen's Method (enhanced) by Jeff Burkey (2024) https://www.mathworks.com/matlabcentral/fileexchange/11190-mann-kendall-tau-b-with-sen-s-method-enhanced was used to calculate the trends. The quality-controlled data generated in this study are publicly available through the Zenodo repository: https://doi.org/10.5281/zenodo.18308385 (Ishaque, 2026).

Acknowledgments

This research was carried out at the Jet Propulsion Laboratory, California Institute of Technology, under a contract with the National Aeronautics and Space Administration (NASA; 80NM0018D0004). This research was funded by NASA through the NASA Sea Level Change Team. We also acknowledge funding support from the Old Dominion University Dorothy Brown Smith Fellowship and Graduate Summer Award to MI. We thank Catherine Schmechtig, Co-chair (France) of BGC-Argo data management task team, for her invaluable assistance with implementing the BGC-Argo quality-control processes for inspecting and correcting bbp and chlorophyll float data. We also thank Lucia Tabacu for generously taking the time to discuss statistical methods most suitable for the analyses presented here.

References

Amol, P., Vinayachandran, P., Shankar, D., Thushara, V., Vijith, V., Chatterjee, A., & Kankonkar, A. (2020). Effect of freshwater advection and winds on the vertical structure of chlorophyll in the northern Bay of Bengal. *Deep Sea Research Part II: Topical Studies in Oceanography*, *179*, 104622. https://doi.org/10.1016/j.dsr2.2019.07.010

Argo. (2026). *Argo float data and metadata from Global Data Assembly Centre (Argo GDAC)*. SEANOE. https://doi.org/10.17882/42182

Barbieux, M., Uitz, J., Gentili, B., Pasqueron de Fommervault, O., Mignot, A., Poteau, A., et al. (2019). Bio-optical characterization of subsurface chlorophyll maxima in the Mediterranean Sea from a Biogeochemical-Argo float database. *Biogeosciences*, *16*(6), 1321–1342. https://doi.org/10.5194/bg-16-1321-2019

Behrenfeld, M. J., Boss, E., Siegel, D. A., & Shea, D. M. (2005). Carbon-based ocean productivity and phytoplankton physiology from space. *Global Biogeochemical Cycles*, *19*(1), 2004GB002299. https://doi.org/10.1029/2004GB002299

Behrenfeld, M. J., O'Malley, R. T., Siegel, D. A., McClain, C. R., Sarmiento, J. L., Feldman, G. C., et al. (2006). Climate-driven trends in contemporary ocean productivity. *Nature*, *444*(7120), 752–755. https://doi.org/10.1038/nature05317

Bendtsen, J., Vives, C. R., & Richardson, K. (2023). Primary production in the North Atlantic estimated from in situ water column data observed by Argo floats and remote sensing. *Frontiers in Marine Science*, *10*, 1062413. https://doi.org/10.3389/fmars.2023.1062413

Bhaskar, T. V. S. U., Swain, D., & Ravichandran, M. (2007). Mixed layer variability in Northern Arabian Sea as detected by an Argo float. *Ocean Science Journal*, *42*(4), 241–246. https://doi.org/10.1007/BF03020915

Bittig, H. C., Maurer, T. L., Plant, J. N., Schmechtig, C., Wong, A. P. S., Claustre, H., et al. (2019). A BGC-Argo Guide: Planning, deployment, data handling and usage. *Frontiers in Marine Science*, *6*, 502. https://doi.org/10.3389/fmars.2019.00502

Boss, E., Picheral, M., Leeuw, T., Chase, A., Karsenti, E., Gorsky, G., et al. (2013). The characteristics of particulate absorption, scattering and attenuation coefficients in the surface ocean; Contribution of the Tara Oceans expedition. *Methods in Oceanography*, *7*, 52–62. https://doi.org/10.1016/j.mio.2013.11.002

Cermeño, P., Dutkiewicz, S., Harris, R. P., Follows, M., Schofield, O., & Falkowski, P. G. (2008). The role of nutricline depth in regulating the ocean carbon cycle. *Proceedings of the National Academy of Sciences*, *105*(51), 20344–20349. https://doi.org/10.1073/pnas.0811302106

Cornec, M., Claustre, H., Mignot, A., Guidi, L., Lacour, L., Poteau, A., et al. (2021). Deep chlorophyll maxima in the global ocean: Occurrences, drivers and characteristics. *Global Biogeochemical Cycles*, *35*(4), e2020GB006759. https://doi.org/10.1029/2020GB006759

Cullen, J. J., & Lewis, M. R. (1995). Biological processes and optical measurements near the sea surface: Some issues relevant to remote sensing. *Journal of Geophysical Research*, *100*(C7), 13255–13266. https://doi.org/10.1029/95JC00454

Currie, J. C., Lengaigne, M., Vialard, J., Kaplan, D. M., Aumont, O., Naqvi, S. W. A., & Maury, O. (2013). Indian Ocean Dipole and El Niño/Southern Oscillation impacts on regional chlorophyll anomalies in the Indian Ocean. *Biogeosciences*, *10*(10), 6677–6698. https://doi.org/10.5194/bg-10-6677-2013

Dalabehara, H., & Sarma, V. (2021). Physical forcing controls spatial variability in primary production in the Indian Ocean. *Deep Sea Research Part II: Topical Studies in Oceanography*, *183*, 104906. https://doi.org/10.1016/j.dsr2.2020.104906

Dall'Olmo, G., Bhaskar Tvs, U., Bittig, H., Boss, E., Brewster, J., Claustre, H., et al. (2019). *BGC Argo quality control manual for particles backscattering* (Version Number: 1.0). Ifremer. https://doi.org/10.13155/60262

Dalpadado, P., Arrigo, K. R., van Dijken, G. L., Gunasekara, S. S., Ostrowski, M., Bianchi, G., & Sperfeld, E. (2021). Warming of the Indian Ocean and its impact on temporal and spatial dynamics of primary production. *Progress in Oceanography*, *198*, 102688. https://doi.org/10.1016/j.pocean.2021.102688

Dave, A. C., & Lozier, M. S. (2013). Examining the global record of interannual variability in stratification and marine productivity in the low-latitude and mid-latitude ocean: Global Stratification and Productivity. *Journal of Geophysical Research: Oceans*, *118*(6), 3114–3127. https://doi.org/10.1002/jgrc.20224

De Boyer Montégut, C., Madec, G., Fischer, A. S., Lazar, A., & Iudicone, D. (2004). Mixed layer depth over the global ocean: An examination of profile data and a profile-based climatology. *Journal of Geophysical Research*, *109*(C12), 2004JC002378. https://doi.org/10.1029/2004JC002378

Dimri, A. P., Allen, S., Huggel, C., Mal, S., Ballesteros-Cánovas, J. A., Rohrer, M., et al. (2021). Climate change, cryosphere and impacts in the Indian Himalayan Region. *Current Science*, *120*(5), 774. https://doi.org/10.18520/cs/v120/i5/774-790

Falkowski, P. G., Barber, R. T., & Smetacek, V. (1998). Biogeochemical controls and feedbacks on ocean primary production. *Science*, *281*(5374), 200–206. https://doi.org/10.1126/science.281.5374.200

Field, C. B., Behrenfeld, M. J., Randerson, J. T., & Falkowski, P. (1998). Primary production of the biosphere: Integrating terrestrial and oceanic components. *Science*, *281*(5374), 237–240. https://doi.org/10.1126/science.281.5374.237

Fox, J., Behrenfeld, M. J., Haëntjens, N., Chase, A., Kramer, S. J., Boss, E., et al. (2020). Phytoplankton growth and productivity in the Western North Atlantic: Observations of regional variability from the NAAMES field campaigns. *Frontiers in Marine Science*, *7*, 24. https://doi.org/10.3389/fmars.2020.00024

Gao, Z., Long, S.-M., Shi, J.-R., Cheng, L., Li, G., & Ying, J. (2023). Indian Ocean mixed layer depth changes under global warming. *Frontiers in Climate*, *5*, 1112713. https://doi.org/10.3389/fclim.2023.1112713

Goes, J. I., Thoppil, P. G., Gomes, H. D. R., & Fasullo, J. T. (2005). Warming of the Eurasian landmass is making the Arabian Sea more productive. *Science*, *308*(5721), 545–547. https://doi.org/10.1126/science.1106610

Graff, J. R., Westberry, T. K., Milligan, A. J., Brown, M. B., Dall'Olmo, G., Dongen-Vogels, V. V., et al. (2015). Analytical phytoplankton carbon measurements spanning diverse ecosystems. *Deep Sea Research Part I: Oceanographic Research Papers*, *102*, 16–25. https://doi.org/10.1016/j.dsr.2015.04.006

Gregg, W. W., Casey, N. W., & McClain, C. R. (2005). Recent trends in global ocean chlorophyll. *Geophysical Research Letters*, *32*(3), L03606. https://doi.org/10.1029/2004GL021808

Gregg, W. W., & Rousseaux, C. S. (2019). Global ocean primary production trends in the modern ocean color satellite record (1998–2015). *Environmental Research Letters*, *14*(12), 124011. https://doi.org/10.1088/1748-9326/ab4667

Hammond, M. L., Beaulieu, C., Henson, S. A., & Sahu, S. K. (2020). Regional surface chlorophyll trends and uncertainties in the global ocean. *Scientific Reports*, *10*(1), 15273. https://doi.org/10.1038/s41598-020-72073-9

Hanson, C. E., Pesant, S., Waite, A. M., & Pattiaratchi, C. B. (2007). Assessing the magnitude and significance of deep chlorophyll maxima of the coastal eastern Indian Ocean. *Deep Sea Research Part II: Topical Studies in Oceanography*, *54*(8–10), 884–901. https://doi.org/10.1016/j.dsr2.2006.08.021

Henson, S. A., Sarmiento, J. L., Dunne, J. P., Bopp, L., Lima, I., Doney, S. C., et al. (2010). Detection of anthropogenic climate change in satellite records of ocean chlorophyll and productivity. *Biogeosciences*, *7*(2), 621–640. https://doi.org/10.5194/bg-7-621-2010

Ishaque, M. (2026). Quality-controlled BGC-Argo data for the Indian Ocean. *Zenodo*. https://doi.org/10.5281/ZENODO.18308385

Izett, R. W., Fennel, K., Stoer, A. C., & Nicholson, D. P. (2023). Reviews and syntheses: Expanding the global coverage of gross primary production and net community production measurements using BGC-Argo floats (preprint). *Biogeochemistry: Open Ocean*. https://doi.org/10.5194/bg-2023-46

Jayaram, C., Bhaskar, T., Chacko, N., Prakash, S., & Rao, K. (2021). Spatio-temporal variability of chlorophyll in the northern Indian Ocean: A biogeochemical Argo data perspective. *Deep Sea Research Part II: Topical Studies in Oceanography*, *183*, 104928. https://doi.org/10.1016/j.dsr2.2021.104928

Jayaram, C., Udaya Bhaskar, T. V. S., Kumar, J. P., & Swain, D. (2019). Cyclone enhanced chlorophyll in the Bay of Bengal as evidenced from satellite and BGC-Argo float observations. *Journal of the Indian Society of Remote Sensing*, *47*(11), 1875–1882. https://doi.org/10.1007/s12524-019-01034-1

Kao, H.-Y., & Yu, J.-Y. (2009). Contrasting Eastern-Pacific and Central-Pacific types of ENSO. *Journal of Climate*, *22*(3), 615–632. https://doi.org/10.1175/2008JCLI2309.1

Keerthi, M. G., Lengaigne, M., Drushka, K., Vialard, J., De Boyer Montegut, C., Pous, S., et al. (2016). Intraseasonal variability of mixed layer depth in the tropical Indian Ocean. *Climate Dynamics*, *46*(7–8), 2633–2655. https://doi.org/10.1007/s00382-015-2721-z

Krishna, M., Prasad, M., Rao, D., Viswanadham, R., Sarma, V., & Reddy, N. (2016). Export of dissolved inorganic nutrients to the northern Indian Ocean from the Indian monsoonal rivers during discharge period. *Geochimica et Cosmochimica Acta*, *172*, 430–443. https://doi.org/10.1016/j.gca.2015.10.013

Kumar, G. S., Prakash, S., Ravichandran, M., & Narayana, A. (2016). Trends and relationship between chlorophyll-*a* and sea surface temperature in the central equatorial Indian Ocean. *Remote Sensing Letters*, *7*(11), 1093–1101. https://doi.org/10.1080/2150704X.2016.1210835

Kumar, S. P., Roshin, R. P., Narvekar, J., Kumar, P. D., & Vivekanandan, E. (2009). Response of the Arabian Sea to global warming and associated regional climate shift. *Marine Environmental Research*, *68*(5), 217–222. https://doi.org/10.1016/j.marenvres.2009.06.010

Kurokawa, J., & Ohara, T. (2020). Long-term historical trends in air pollutant emissions in Asia: Regional Emission inventory in ASia (REAS) version 3. *Atmospheric Chemistry and Physics*, *20*(21), 12761–12793. https://doi.org/10.5194/acp-20-12761-2020

Kuttippurath, J., Maishal, S., Anjaneyan, P., Sunanda, N., & Chakraborty, K. (2023). Recent changes in atmospheric input and primary productivity in the north Indian Ocean. *Heliyon*, *9*(7), e17940. https://doi.org/10.1016/j.heliyon.2023.e17940

Lakshmi, R. S., Chatterjee, A., Prakash, S., & Mathew, T. (2020). Biophysical interactions in driving the summer monsoon chlorophyll bloom off the Somalia Coast. *Journal of Geophysical Research: Oceans*, *125*(3), e2019JC015549. https://doi.org/10.1029/2019JC015549

Li, G., Cheng, L., Zhu, J., Trenberth, K. E., Mann, M. E., & Abraham, J. P. (2020). Increasing ocean stratification over the past half-century. *Nature Climate Change*, *10*(12), 1116–1123. https://doi.org/10.1038/s41558-020-00918-2

Löscher, C. R. (2021). Reviews and syntheses: Trends in primary production in the Bay of Bengal—Is it at a tipping point? *Biogeosciences*, *18*(17), 4953–4963. https://doi.org/10.5194/bg-18-4953-2021

Mahala, B. K., Nayak, B. K., & Mohanty, P. K. (2015). Impacts of ENSO and IOD on tropical cyclone activity in the Bay of Bengal. *Natural Hazards*, *75*(2), 1105–1125. https://doi.org/10.1007/s11069-014-1360-8

Malsang, M., Resplandy, L., Bopp, L., Zhao, Y., Ditkovsky, S., Yang, F., et al. (2024). Contemporary decline in northern Indian Ocean primary production offset by rising atmospheric nitrogen deposition. *Frontiers in Marine Science*, *11*, 1418634. https://doi.org/10.3389/fmars.2024.1418634

Martinez, E., Antoine, D., D'Ortenzio, F., & Gentili, B. (2009). Climate-driven basin-scale decadal oscillations of oceanic phytoplankton. *Science*, *326*(5957), 1253–1256. https://doi.org/10.1126/science.1177012

Masuda, Y., Yamanaka, Y., Smith, S. L., Hirata, T., Nakano, H., Oka, A., & Sumata, H. (2021). Photoacclimation by phytoplankton determines the distribution of global subsurface chlorophyll maxima in the ocean. *Communications Earth & Environment*, *2*(1), 128. https://doi.org/10.1038/s43247-021-00201-y

McCluskey, E., Brewin, R. J. W., Vanhellemont, Q., Jones, O., Cummings, D., Tilstone, G., et al. (2022). On the seasonal dynamics of phytoplankton chlorophyll-a concentration in nearshore and offshore waters of plymouth, in the English Channel: Enlisting the help of a surfer. *Oceans*, *3*(2), 125–146. https://doi.org/10.3390/oceans3020011

McPhaden, M. J., Zebiak, S. E., & Glantz, M. H. (2006). ENSO as an integrating concept in Earth science. *Science*, *314*(5806), 1740–1745. https://doi.org/10.1126/science.1132588

Mignot, A., Claustre, H., Uitz, J., Poteau, A., D'Ortenzio, F., & Xing, X. (2014). Understanding the seasonal dynamics of phytoplankton biomass and the deep chlorophyll maximum in oligotrophic environments: A Bio-Argo float investigation. *Global Biogeochemical Cycles*, *28*(8), 856–876. https://doi.org/10.1002/2013GB004781

Modi, A., & Koll, R. M. (2023). Past trends and future projections of marine primary productivity in the tropical Indian Ocean. In S. C. Tripathy & A. Singh (Eds.), *Dynamics of planktonic primary productivity in the Indian Ocean* (pp. 191–206). Springer International Publishing. https://doi.org/10.1007/978-3-031-34467-1_9

Morel, A., Huot, Y., Gentili, B., Werdell, P. J., Hooker, S. B., & Franz, B. A. (2007). Examining the consistency of products derived from various ocean color sensors in open ocean (Case 1) waters in the perspective of a multi-sensor approach. *Remote Sensing of Environment*, *111*(1), 69–88. https://doi.org/10.1016/j.rse.2007.03.012

Pandey, S., Bhagawati, C., Dandapat, S., & Chakraborty, A. (2019). Surface chlorophyll anomalies associated with Indian Ocean Dipole and El Niño Southern Oscillation in North Indian Ocean: A case study of 2006–2007 event. *Environmental Monitoring and Assessment*, *191*(S3), 807. https://doi.org/10.1007/s10661-019-7754-z

Pedde, S., Kroeze, C., Mayorga, E., & Seitzinger, S. P. (2017). Modeling sources of nutrients in rivers draining into the Bay of Bengal—A scenario analysis. *Regional Environmental Change*, *17*(8), 2495–2506. https://doi.org/10.1007/s10113-017-1176-7

Pervez, M. S., & Henebry, G. M. (2015). Spatial and seasonal responses of precipitation in the Ganges and Brahmaputra river basins to ENSO and Indian Ocean dipole modes: Implications for flooding and drought. *Natural Hazards and Earth System Sciences*, *15*(1), 147–162. https://doi.org/10.5194/nhess-15-147-2015

Peter, B. N., Sreejith, M., & Siswanto, E. (2022). Variability of Arabian Sea surface circulation and chlorophyll distribution: A remote sensing estimation. *Terrestrial, Atmospheric and Oceanic Sciences*, *33*(1), 22. https://doi.org/10.1007/s44195-022-00024-0

Prakash, S., Nair, T. B., Bhaskar, T. U., Prakash, P., & Gilbert, D. (2012). Oxycline variability in the central Arabian Sea: An Argo-oxygen study. *Journal of Sea Research*, *71*, 1–8. https://doi.org/10.1016/j.seares.2012.03.003

Prakash, S., & Ramesh, R. (2007). Is the Arabian Sea getting more productive?

Prasanna Kumar, S., Muraleedharan, P. M., Prasad, T. G., Gauns, M., Ramaiah, N., de Souza, S. N., et al. (2002). Why is the Bay of Bengal less productive during summer monsoon compared to the Arabian Sea? The Bay of Bengal less productive during summer monsoon. *Geophysical Research Letters*, *29*(24), 88-1–4. https://doi.org/10.1029/2002GL016013

Prasanna Kumar, S., Narvekar, J., Nuncio, M., Gauns, M., & Sardesai, S. (2009). What drives the biological productivity of the northern Indian Ocean? In J. D. Wiggert, R. R. Hood, S. W. A. Naqvi, K. H. Brink, & S. L. Smith (Eds.), *Geophysical monograph series* (Vol. 185, pp. 33–56). American Geophysical Union. https://doi.org/10.1029/2008GM000757

Richardson, K., & Bendtsen, J. (2019). Vertical distribution of phytoplankton and primary production in relation to nutricline depth in the open ocean. *Marine Ecology Progress Series*, *620*, 33–46. https://doi.org/10.3354/meps12960

Roesler, C., Uitz, J., Claustre, H., Boss, E., Xing, X., Organelli, E., et al. (2017). Recommendations for obtaining unbiased chlorophyll estimates from in situ chlorophyll fluorometers: A global analysis of WET Labs ECO sensors. *Limnology and Oceanography: Methods*, *15*(6), 572–585. https://doi.org/10.1002/lom3.10185

Roxy, M. K., Gnanaseelan, C., Parekh, A., Chowdary, J. S., Singh, S., Modi, A., et al. (2020). Indian Ocean warming. In R. Krishnan, J. Sanjay, C. Gnanaseelan, M. Mujumdar, A. Kulkarni, & S. Chakraborty (Eds.), *Assessment of climate change over the indian region: A report of the ministry of Earth sciences (MoES), government of India* (pp. 191–206). Springer Singapore. https://doi.org/10.1007/978-981-15-4327-2_10

Roxy, M. K., Ritika, K., Terray, P., & Masson, S. (2014). The curious case of Indian Ocean Warming. *Journal of Climate*, *27*(22), 8501–8509. https://doi.org/10.1175/JCLI-D-14-00471.1

Roxy, M. K., Modi, A., Murtugudde, R., Valsala, V., Panickal, S., Prasanna Kumar, S., et al. (2016). A reduction in marine primary productivity driven by rapid warming over the tropical Indian Ocean. *Geophysical Research Letters*, *43*(2), 826–833. https://doi.org/10.1002/2015GL066979

Saji, N., & Yamagata, T. (2003). Possible impacts of Indian Ocean Dipole mode events on global climate. *Climate Research*, *25*, 151–169. https://doi.org/10.3354/cr025151

Saji, N. H., Goswami, B. N., Vinayachandran, P. N., & Yamagata, T. (1999). A dipole mode in the tropical Indian Ocean. *Nature*, *401*(6751), 360–363. https://doi.org/10.1038/43854

Sankar, S., Thondithala Ramachandran, A., Franck Eitel, K. G., Kondrik, D., Sen, R., Madipally, R., & Pettersson, L. H. (2019). The influence of tropical Indian Ocean warming and Indian Ocean Dipole on the surface chlorophyll concentration in the eastern Arabian Sea (preprint). *Earth System Science/Response to Global Change: Climate Change*. https://doi.org/10.5194/bg-2019-169

Sarma, V. V. S. S., Sridevi, B., Kumar, A., Bikkina, S., Kumari, V. R., Bikkina, P., et al. (2022). Impact of atmospheric anthropogenic nitrogen on new production in the northern Indian Ocean: Constrained based on satellite aerosol optical depth and particulate nitrogen levels. *Environmental Science: Processes & Impacts*, *24*(10), 1895–1911. https://doi.org/10.1039/D2EM00234E

Sathyendranath, S., Brewin, R., Brockmann, C., Brotas, V., Calton, B., Chuprin, A., et al. (2019). An ocean-colour time series for use in climate studies: The experience of the ocean-colour climate change initiative (OC-CCI). *Sensors*, *19*(19), 4285. https://doi.org/10.3390/s19194285

Schmechtig, C., Claustre, H., Poteau, A., & D'Ortenzio, F. (2018). *Bio-Argo quality control manual for the Chlorophyll-A concentration* (Version Number: 1.1). Ifremer. https://doi.org/10.13155/35385

Shafeeque, M., George, G., Akash, S., Smitha, B., Shah, P., & Balchand, A. (2021). Interannual variability of chlorophyll-a and impact of extreme climatic events in the South Eastern Arabian Sea. *Regional Studies in Marine Science*, *48*, 101986. https://doi.org/10.1016/j.rsma.2021.101986

Siegel, D. A., Buesseler, K. O., Doney, S. C., Sailley, S. F., Behrenfeld, M. J., & Boyd, P. W. (2014). Global assessment of ocean carbon export by combining satellite observations and food-web models. *Global Biogeochemical Cycles*, *28*(3), 181–196. https://doi.org/10.1002/2013GB004743

Singh, A., Gandhi, N., & Ramesh, R. (2012). Contribution of atmospheric nitrogen deposition to new production in the nitrogen limited photic zone of the northern Indian Ocean. *Journal of Geophysical Research*, *117*(C6), 2011JC007737. https://doi.org/10.1029/2011JC007737

Siswanto, E., Sarker, M. L. R., Peter, B. N., Takemura, T., Horii, T., Matsumoto, K., et al. (2023). Variations of phytoplankton chlorophyll in the Bay of Bengal: Impact of climate changes and nutrients from different sources. *Frontiers in Marine Science*, *10*, 1052286. https://doi.org/10.3389/fmars.2023.1052286

Somavilla, R., Rodriguez, C., Lavín, A., Viloria, A., Marcos, E., & Cano, D. (2019). Atmospheric control of deep chlorophyll maximum development. *Geosciences*, *9*(4), 178. https://doi.org/10.3390/geosciences9040178

Sridevi, B., Sabira, S., & Sarma, V. (2023). Impact of ocean warming on net primary production in the northern Indian Ocean: Role of aerosols and freshening of surface ocean. *Environmental Science and Pollution Research*, *30*(18), 53616–53634. https://doi.org/10.1007/s11356-023-26001-9

Stramska, M., & Cieszyńska, A. (2015). Ocean colour estimates of particulate organic carbon reservoirs in the global ocean—Revisited. *International Journal of Remote Sensing*, *36*(14), 3675–3700. https://doi.org/10.1080/01431161.2015.1049380

Strutton, P. G., Trull, T. W., Phillips, H. E., Duran, E. R., & Pump, S. (2023). Biogeochemical Argo floats reveal the evolution of subsurface chlorophyll and particulate organic carbon in Southeast Indian Ocean eddies. *Journal of Geophysical Research: Oceans*, *128*(4), e2022JC018984. https://doi.org/10.1029/2022JC018984

Su, J., Strutton, P. G., & Schallenberg, C. (2021). The subsurface biological structure of Southern Ocean eddies revealed by BGC-Argo floats. *Journal of Marine Systems*, *220*, 103569. https://doi.org/10.1016/j.jmarsys.2021.103569

Sun, Y., Gao, P., Tariq, S., Azhar, A., Haq, Z. U., & Mehmood, U. (2023). Assessment of long-term trends in chlorophyll-a and sea surface temperature in the Arabian Sea and their association with aerosols using remote sensing. *Ocean & Coastal Management*, *242*, 106716. https://doi.org/10.1016/j.ocecoaman.2023.106716

Sunanda, N., Kuttippurath, J., Chakraborty, A., & Peter, R. (2023). Stressors of primary productivity in the north Indian Ocean revealed by satellite, reanalysis and CMIP6 data. *Progress in Oceanography*, *219*, 103164. https://doi.org/10.1016/j.pocean.2023.103164

Syroka, J., & Toumi, R. (2004). On the withdrawal of the Indian summer monsoon. *Quarterly Journal of the Royal Meteorological Society*, *130*(598), 989–1008. https://doi.org/10.1256/qj.03.36

Thushara, V., & Vinayachandran, P. N. (2020). Unprecedented surface chlorophyll blooms in the Southeastern Arabian Sea during an extreme negative Indian Ocean dipole. *Geophysical Research Letters*, *47*(13), e2019GL085026. https://doi.org/10.1029/2019GL085026

Thushara, V., Vinayachandran, P. N. M., Matthews, A. J., Webber, B. G. M., & Queste, B. Y. (2019). Vertical distribution of chlorophyll in dynamically distinct regions of the southern Bay of Bengal. *Biogeosciences*, *16*(7), 1447–1468. https://doi.org/10.5194/bg-16-1447-2019

Varna, M., Singh, A., Sahoo, D., & Sengupta, D. (2021). Strengthening of basin-scale ocean currents in winter drives decadal salinity decline in the Eastern Arabian Sea. *Geophysical Research Letters*, *48*(16), e2021GL094516. https://doi.org/10.1029/2021GL094516

Vinaya Kumari, P., Jayappa, K. S., Thomas, S., & Gupta, A. (2021). Decadal variations of sea surface temperature in the eastern Arabian Sea and its impacts on the net primary productivity. *Spatial Information Research*, *29*(2), 137–148. https://doi.org/10.1007/s41324-020-00340-y

Westberry, T., Behrenfeld, M. J., Siegel, D. A., & Boss, E. (2008). Carbon-based primary productivity modeling with vertically resolved photoacclimation. *Global Biogeochemical Cycles*, *22*(2), 2007GB003078. https://doi.org/10.1029/2007GB003078

Wolter, K., & Timlin, M. S. (2011). El Niño/Southern Oscillation behaviour since 1871 as diagnosed in an extended multivariate ENSO index (MEI.ext). *International Journal of Climatology*, *31*(7), 1074–1087. https://doi.org/10.1002/joc.2336

Xing, X., Claustre, H., Blain, S., D'Ortenzio, F., Antoine, D., Ras, J., & Guinet, C. (2012). Quenching correction for in vivo chlorophyll fluorescence acquired by autonomous platforms: A case study with instrumented elephant seals in the Kerguelen region (Southern Ocean): Quenching correction for chlorophyll fluorescence. *Limnology and Oceanography: Methods*, *10*(7), 483–495. https://doi.org/10.4319/lom.2012.10.483

Xu, Y., Wu, Y., Wang, H., Zhang, Z., Li, J., & Zhang, J. (2021). Seasonal and interannual variabilities of chlorophyll across the eastern equatorial Indian Ocean and Bay of Bengal. *Progress in Oceanography*, *198*, 102661. https://doi.org/10.1016/j.pocean.2021.102661

Yamaguchi, R., & Suga, T. (2019). Trend and variability in global upper-ocean stratification since the 1960s. *Journal of Geophysical Research: Oceans*, *124*(12), 8933–8948. https://doi.org/10.1029/2019JC015439

Yang, B., Fox, J., Behrenfeld, M. J., Boss, E. S., Haëntjens, N., Halsey, K. H., et al. (2021). In situ estimates of net primary production in the Western North Atlantic with argo profiling floats. *Journal of Geophysical Research: Biogeosciences*, *126*(2), e2020JG006116. https://doi.org/10.1029/2020JG006116

Yang, B., Gomez, F., Schmid, C., & Baringer, M. (2022). In situ estimates of net primary production in the open-ocean Gulf of Mexico. *Limnology and Oceanography Letters*, *7*(5), 427–434. https://doi.org/10.1002/lol2.10270

Yin, Z., Dong, Q., Xiang, K., & Bian, M. (2022). Seasonal evolution of Chlorophyll-a in the North Indian Ocean associated with the Indian Ocean dipole and two types of El Niño events. *Journal of Marine Science and Engineering*, *10*(7), 997. https://doi.org/10.3390/jmse10070997

Zhang, T., Hoell, A., Perlwitz, J., Eischeid, J., Murray, D., Hoerling, M., & Hamill, T. M. (2019). Towards probabilistic multivariate ENSO monitoring. *Geophysical Research Letters*, *46*(17–18), 10532–10540. https://doi.org/10.1029/2019GL083946